ORIGINAL ARTICLE

Understanding the variation of stratosphere–troposphere coupling during stratospheric northern annular mode events from a mass circulation perspective

Yueyue Yu[1,2] · Rongcai Ren[1,2]

Abstract

We revisit the various stratosphere–troposphere coupling relation from the perspective of the meridional mass circulation. We constructed 10-hPa northern annular mode (NAM) phase composites to show the typical spatiotemporal evolution of circulation anomalies during the NAM's life cycle. Our results indicate that there is large case-to-case difference in the temporal evolution and vertical profile of polar temperature anomalies during NAM events, which shows no strong dependence on the intensity and duration of NAM events, but agrees well with the variations of the three branches of mass circulation at 60°N: the stratospheric poleward warm air branch (ST), the poleward warm air branch in the upper troposphere (WB), and the equatorward cold air branch in the lower troposphere (CB). Such correspondence is due to the dynamic heating and cooling anomalies associated with the redistribution of air masses by the anomalous meridional mass circulation in different isentropic layers. The various relationship among the three mass circulation branches is attributed to anomalous wave activities. The amplitude and westward tilt of waves are always stronger (weaker) throughout the stratosphere before (after) the peak time of negative NAM events, leading to a stronger (weaker) ST before (after) the peak time. Variations in WB and CB are mostly dependent on wave variabilities in the mid- to lower troposphere, leading to variations in the timing of in- or out-of-phase coupling of the ST with the WB and CB, and thus various thermostructure during NAM events. At a later stage of the negative NAM events when the polar temperature becomes colder and the polar jet recovers, the weakened baroclinic instability in the lower stratosphere provides favorable conditions for the strengthening of the WB and CB if wave activities strengthen in the troposphere during that period.

✉ Rongcai Ren
rrc@lasg.iap.ac.cn

1 Key Laboratory of Meteorological Disaster, Ministry of Education (KLME), Joint International Research Laboratory of Climate and Environment Change (ILCEC), Collaborative Innovation Center on Forecast and Evaluation of Meteorological Disasters (CIC-FEMD), Nanjing University of Information Science and Technology, Nanjing 210044, China

2 State Key Laboratory of Numerical Modeling for Atmospheric Sciences and Geophysical Fluid Dynamics (LASG), Institute of Atmospheric Physics, Chinese Academy of Sciences, Beijing 100029, China

1 Introduction

The pioneering work of Thompson and Wallace (1998) and Baldwin and Dunkerton (1999) on the quasi-annular mode of atmospheric variability in the northern hemisphere winter—the northern annular mode (NAM)—has had a huge impact on our understanding of stratosphere–troposphere coupling (S–T coupling). The negative (positive) phase of the stratospheric NAM corresponds to a weaker (stronger) and warmer (colder) stratospheric polar vortex with larger (smaller) amplitudes of wave flow surrounding the polar region (Kuroda 2002; Zhou et al. 2002; Limpasuvan et al. 2004). At the Earth's surface, the NAM is linked to the Arctic Oscillation/North Atlantic Oscillation (AO/NAO) and is characterized by the downward propagation of extra-tropical anomalies (Kodera and Kuroda 1990, 2000a; Baldwin and Dunkerton 1999, 2001; Coughlin and Tung 2005). In this way, the NAM links the wintertime polar vortex oscillation in the stratosphere and connects to the

AO/NAO and, as a consequence, affects the weather in the troposphere (Rind et al. 2005; Scaife et al. 2005; Thompson et al. 2005; Kolstad and Charlton-Perez 2011; Hardiman et al. 2012). This downward influence potentially leads to improved weather predictions after significant perturbations of the stratospheric polar vortex (Baldwin et al. 2003; Hardiman et al. 2011; Sigmond et al. 2013).

The most common explanation for this downward propagation of stratospheric perturbations is the interaction between changes in the conditions for planetary wave propagation as a result of changes in the zonal mean flow (Shindell et al. 1999; Plumb and Semeniuk 2002; Holton 2004; Limpasuvan et al. 2004, 2005). Planetary Rossby waves generated in the troposphere propagate upward and, when they grow large enough to break up and be absorbed, they can change the stratospheric flow. The region where there is the strongest interaction between the waves and the mean flow shifts slightly due to these changes in the basic state, resulting in a downward and poleward progression of the mean flow perturbations. A different mechanism—the downward reflection of wave energy by the stratosphere back into the troposphere—has been suggested as a mechanism by which the stratosphere can affect the troposphere (Hines 1974; Geller and Alpert 1980; Schmitz and Grieger 1980). An observational study using new dynamic and statistical diagnostics found evidence for such a reflection in the upper stratosphere of the northern hemisphere, which exerts an impact on the structure of tropospheric waves of zonal wavenumber 1 (Perlwitz and Harnik 2004). The main basic state configuration under which the reflection of wavenumber 1 occurs is when the stratospheric jet peaks in the mid-stratosphere (Harnik and Lindzen 2001; Perlwitz and Harnik 2004).

A large case-to-case variability in the strength of the downward propagation of the anomaly signals is found after weak or strong stratospheric polar vortex events. Baldwin and Dunkerton (1999) noticed that not all NAM anomalies in the upper stratosphere propagate downward, even in low-pass filtered data. Some extreme stratospheric events induce anomalies in the AO/NAO and some do not (Kodera and Kuroda 2000a; Nakagawa and Yamazaki 2006; Gerber et al. 2009). Runde et al. (2016) showed that no significant tropospheric response can be detected in about 80% of all anomalous strong and weak stratospheric polar vortex events. Cai and Ren (2006, 2007), Ren and Cai (2007) reported that the beginning of the equatorward propagation of the tropospheric temperature anomalies in high latitudes coincides with the arrival of poleward- and downward-propagating temperature anomalies of the opposite sign in the stratosphere. In other words, the downward propagation of isentropic temperature anomalies into the troposphere is discontinuous at high latitudes.

Whether the stratospheric signals can propagate or have a significant impact on the troposphere and surface has been found to be related to the properties of the stratospheric perturbation (e.g., the timing of the winter season, and the persistence, intensity, and wave scale of the perturbation). Kodera and Kuroda (2000a) showed that downward propagation from the stratosphere toward the troposphere tends to occur in late winter/spring, but not during fall/early winter. Baldwin and Dunkerton (1999) showed that only those perturbations with a large amplitude and persistence have a clear signature throughout the troposphere. Numerical model simulations (e.g., Yoden et al. 1999; Perlwitz and Graf 2001) also found that the strength of the polar vortex is a key factor in the downward effects of the stratosphere on tropospheric circulation, particularly for zonal wavenumber 1. Runde et al. (2016) confirmed that the stratospheric perturbation of both weak and strong events with a significant tropospheric response persists significantly longer throughout the stratosphere than events without a tropospheric response, but argued that the strength of the stratospheric perturbation determines the strength of the tropospheric response to only a small degree. Hitchcock et al. (2013) found that the tropospheric impact of a weak vortex event followed by the temperature anomalies characteristic of the polar night jet oscillation events is stronger and more coherent than that of non-polar night jet oscillation events. Recent studies have emphasized the role of tropospheric eddy feedback on the downward propagation of stratospheric anomalies on both synoptic (Domeisen et al. 2013) and planetary scales (Hitchcock and Simpson 2014). Zhou et al. (2002), Song and Robinson (2006), and Nakagawa and Yamazaki (2006) reported that tropospheric wave forcing is essential to produce the tropospheric anomalies. If the initial wave forcing from the troposphere is strong and persistent enough to reverse the polar westerlies, then the warm anomalies can descend along with the critical line. However, if the change in the mean state is not large enough to affect wave propagation, we do not see downward propagation. Therefore, there is still an open question as to the extent to which the large case-to-case variability in the tropospheric response is determined by the properties of the stratospheric perturbation, or whether this is due to the internal variability of the troposphere (which might randomly mask the response) and the state of the troposphere before or during the stratospheric influences.

There are various criteria to determine whether a stratospheric NAM event can be transmitted to the troposphere or surface. Most studies have selected extreme strong and weak NAM events, among which the extreme weak events always correspond to sudden warming of the stratosphere (SSW). Kodera and Kuroda (2000b) categorized the vertical structures of the AO into two types depending on whether it is accompanied by the downward propagation of zonal mean temperature anomalies from the stratosphere. Hitchcock

et al. (2013) classified SSW events based on whether a polar jet oscillation is followed, namely an extended recovery phase characterized by a persistent lower stratospheric warm anomaly and a cold anomaly that forms in the mid- to upper stratosphere and then descends. Zhou et al. (2002) defined a propagating (non-propagating) warming event as one in which a temperature anomaly greater than two standard deviations at 10 hPa is followed by a temperature anomaly greater than 1.5 standard deviations (smaller than one standard deviation) at 200 hPa. Runde et al. (2016) classified stratospheric sudden warming events based on the time series of the detrended 90-day low-pass filtered polar geopotential height anomaly at each level from 30 to 700 hPa: if a threshold exceedance above 1.5 standard deviations following the stratospheric central day was found at all these levels, the event was classified as a stratospheric extreme event with a significant tropospheric response; otherwise, the event was classified as a non-significant tropospheric response event. These various definitions attempted to separate propagating and non-propagating events, but they are still arbitrary—for example, they do not define the exact time period after the stratospheric central day on which the tropospheric anomalies are chosen to determine the type, nor the optimum tropospheric reference level.

This study aims to objectively present the diversity of S–T variation during stratospheric NAM events from the perspective of mass circulation. As shown by Johnson and coworkers (Gallimore and Johnson 1981; Townsend and Johnson 1985; Johnson 1989), the global meridional circulation is essentially a Hadley-type mass circulation from the equator to the poles forced by both diabatic heating/cooling and eddy-induced forcing. The global meridional circulation is composed of poleward mass transport in the upper isentropic layers (the warm air branch) and an equatorward mass transport in the lower isentropic layers (the cold air branch). In the framework of mass circulation, Yu et al. (2014) conducted a mass budget analysis over the polar region and found that when winter-mean Arctic surface pressure anomalies are positive, both the cold and warm mass circulation branches tend to strengthen, and the variation of the stratospheric portion of the warm air branch leads that of the mass circulation branches in the troposphere, giving rise to more mass anomalies transported in, which can explain the mass source of the winter-mean Arctic surface pressure anomalies. Yu et al. (2018a, c) reported the dominant role of the adiabatic mass transport across the polar circle in changing to the polar mass/pressure/height in the polar stratosphere, which is closely related with stratospheric NAM variability and SSW events. Yu et al. (2015a, b, c), Iwasaki and Mochizuki (2012), Iwasaki et al. (2014) and Shoji et al. (2014) showed that the timing of cold air outbreaks in mid-latitudes are associated with the strengthening of the equatorward transport of a cold air mass in the lower

troposphere via the redistribution of the polar cold air mass. The changes in the amount of the air mass below 270 K in mid-latitudes lead to changes in the surface air temperature. They further found that the equatorward cold air branch near the surface is almost synchronized with the poleward transport of warm air in the upper atmosphere (including the stratosphere) into the polar region. The meridional mass transport in the stratospheric layers (a portion of the warm branch) and the cold branch also have a significant positive correlation, though their relation is slightly weaker and shows some time lag as a result of the wave-filtering effect of the stratosphere (Cai et al. 2016). Thus investigating the S–T relationships in the perspective of the variabilities of the warm and cold branches of the meridional mass circulation might provide richer information and a better understanding of the uncertainties in the downward propagation of stratospheric anomalies and the associated impacts on weather.

This paper is organized as follows. Section 2 describes the dataset used and the methodology for calculating the mass circulation variables, the pressure torque and drag, the wave indices, the selection method for NAM events, and the composite method based on the phase of the life cycle of the NAM events (the NAM phase composites). In Sect. 3, we first examine the case-to-case variability of anomalies in the polar mean temperature and the vertical structure of the meridional mass circulation at the polar circle in each NAM event and then identify the leading types of S–T variation based on the variations in the stratospheric warm branch and the tropospheric branches of the meridional circulation. Section 3 also discusses the temporal evolution of the temperature, mass, and adiabatic/diabatic mass circulation anomalies in NAM events belonging to different types of S–T variation. We show that the typical propagating features of polar temperature anomalies around NAM events (including not only whether, but also when, the anomaly signals propagate to the troposphere) are due to the redistribution of cold and warm air mass by the various coupling combinations of the meridional mass circulation branches in the stratosphere and troposphere. The amplitude of westward titling of waves responsible for the variation in the mass circulation and thus S–T variation are investigated in Sect. 4 and our conclusions are presented in Sect. 5.

2 Data and methods

2.1 Data

The data used in this study include the daily surface air temperature (SAT), the surface pressure (P_s), the surface meridional wind (v_s), and the three-dimensional air temperature (T), meridional wind (v), and zonal wind (u) fields derived from the six-hourly ERA-Interim dataset from January 1979

to December 2011 (ECMWF 2012; Simmons et al. 2006; Dee et al. 2011). The data fields are on $1.5° \times 1.5°$ grids and there are 37 pressure levels from 1000 to 1 hPa. The three-dimensional and surface potential temperature (θ and θ_s) fields are derived from daily fields of the SAT, T, and P_s.

2.2 Variables associated with mass circulation

We strictly followed Yu et al. (2014) (also see Pauluis et al. 2008; Cai and Shin 2014; Yu et al. 2015b) to calculate the variables associated with meridional mass circulation, including the zonally integrated air mass (M) and its tendency (dM/dt), and the adiabatic/meridional mass fluxes (F_{ad}) in isentropic layers and the diabatic/vertical mass fluxes (F_d) across isentropic levels from the daily fields. All these variables are functions of latitude, potential temperature, and time. We preselected 15 potential temperature surfaces Θ_n ($n = 1–15$): 260, 270, 280, 290, 300, 315, 330, 350, 370, 400, 450, 550, 650, 850, and 1200 K. All mass circulation variables except F_d are defined in the 14 layers between the Θ_n and Θ_{n+1} surfaces, plus two additional layers: (1) the surface layer, which accounts for all the mass between the ground and the minimum of Θ_n that satisfies $\Theta_n > \Theta_s$; and (2) the top layer, which accounts for all the air mass above 1200 K. We use the bottom surface of each layer (Θ_n for the layer between Θ_n and Θ_{n+1} and Θ_s for the surface layer) to reference the variables defined in these isentropic layers. By contrast, the diabatic mass flux across isentropic levels (F_d) is defined at all Θ_n that satisfy $\Theta_n > \Theta_s$, where Θ_s is the surface potential temperature varying with location and time (note that the mass flux across Θ_s is always zero because we only considered the dry air mass in this study). We then applied the method of Lagrangian multipliers according to Shin (2012) to obtain a self-consistent mass budget on a daily basis that roughly met the following constraints: (1) the mass tendency in the isentropic tube along latitude was equal to the adiabatic and diabatic mass flux convergence; (2) there was no net mass loss or gain due to adiabatic mass transport in a global isentropic layer; and (3) there was no diabatic mass flux into an atmospheric column from the surface and from the top of the atmosphere (see details in Yu et al. 2014).

Positive (negative) values of F_d correspond to upward mass fluxes across the isentropic surface due to diabatic heating (cooling). Positive values of F_d are mainly observed in tropical regions and in the surface layer in the extra-tropics, whereas negative values are found above the surface layer in the extra-tropics (see Cai and Shin 2014, Fig. 1b). Positive (negative) values of F_{ad} correspond to poleward (equatorward) mass transport across latitude within the two adjacent isentropic surfaces. Negative values of F_{ad} mainly appear in the lower troposphere within the equatorward cold air branch of the meridional mass circulation, whereas positive values mainly appear in the upper layers within the poleward warm air branch (see Cai and Shin 2014, Fig. 1a).

We next define the intensity of the stratospheric portion of the warm air branch (ST) at the polar circle (60°N) as the sum of F_{ad} above 400 K. We define the intensity of the poleward warm air branch in the upper troposphere (WB) at 60°N as the sum of F_{ad} from the separating level Θ_n^* to 370 K. We define the intensity of the equatorward cold air branch in the lower troposphere (CB) at 60°N as the negative sum of F_{ad} below the separating level Θ_n^* for that latitude. The level that separates the warm and cold branches at 60°N and at each day t is identified by searching for the isentropic level Θ_n^*, such that the vertical sum of F_{ad} from the base to all Θ_n, Θ_n^* reaches its maximum negative value. The value of Θ_n^* varies from day to day, but mainly lies between 270 and 290 K around 60°N.

In this study, we also calculated the accumulated mass (M_{accum}), which is defined as the sum of the isentropic layer mass above each isentropic surface. By definition, the M_{accum} at isentropic level 260 K is equal to the total air mass in the column, proportional to the surface pressure, while at other isentropic levels above 260 K, M_{accum} is proportional to the pressure there. In addition, we linearly interpolate the temperature fields in the pressure levels into isentropic levels—that is, 260, 270, 280, 290, 300, 315, 330, 350, 370, 400, 450, 550, 650, 850, and 1200 K—for easy comparison with the variability of the mass circulation. Note that the temperature in isentropic levels is directly related to the pressure or the total air mass above a given level according to the definition of potential temperature. Thus the coupling or decoupling relationship between different branches of meridional mass circulation is expected to physically explain the vertical–latitudinal variations in temperature and pressure/geopotential height by redistributing the layer mass.

2.3 Variables describing the wave properties

We derive two indices of wave properties related to the strength of the poleward mass transport into the polar stratosphere: the wave amplitude and the vertical westward tilting of waves along 60°N. Following Zhang et al. (2013), the wave amplitude index at pressure level p and time t is defined as the root mean square of the zonal deviations of geopotential height. Larger values of the wave amplitude index represent a higher zonal asymmetry of the geopotential height field or a larger wave amplitude, and vice versa. In addition, the westward tilting index is derived based on the effective phase difference between the temperature field and the geopotential field following Yu et al. (2018a) and Cai et al. (2014). Positive values of the westward tilting index indicate vertically westward-tilted waves—that is, the temperature troughs (ridges) are on the west side of the geopotential height troughs (ridges) and negative values
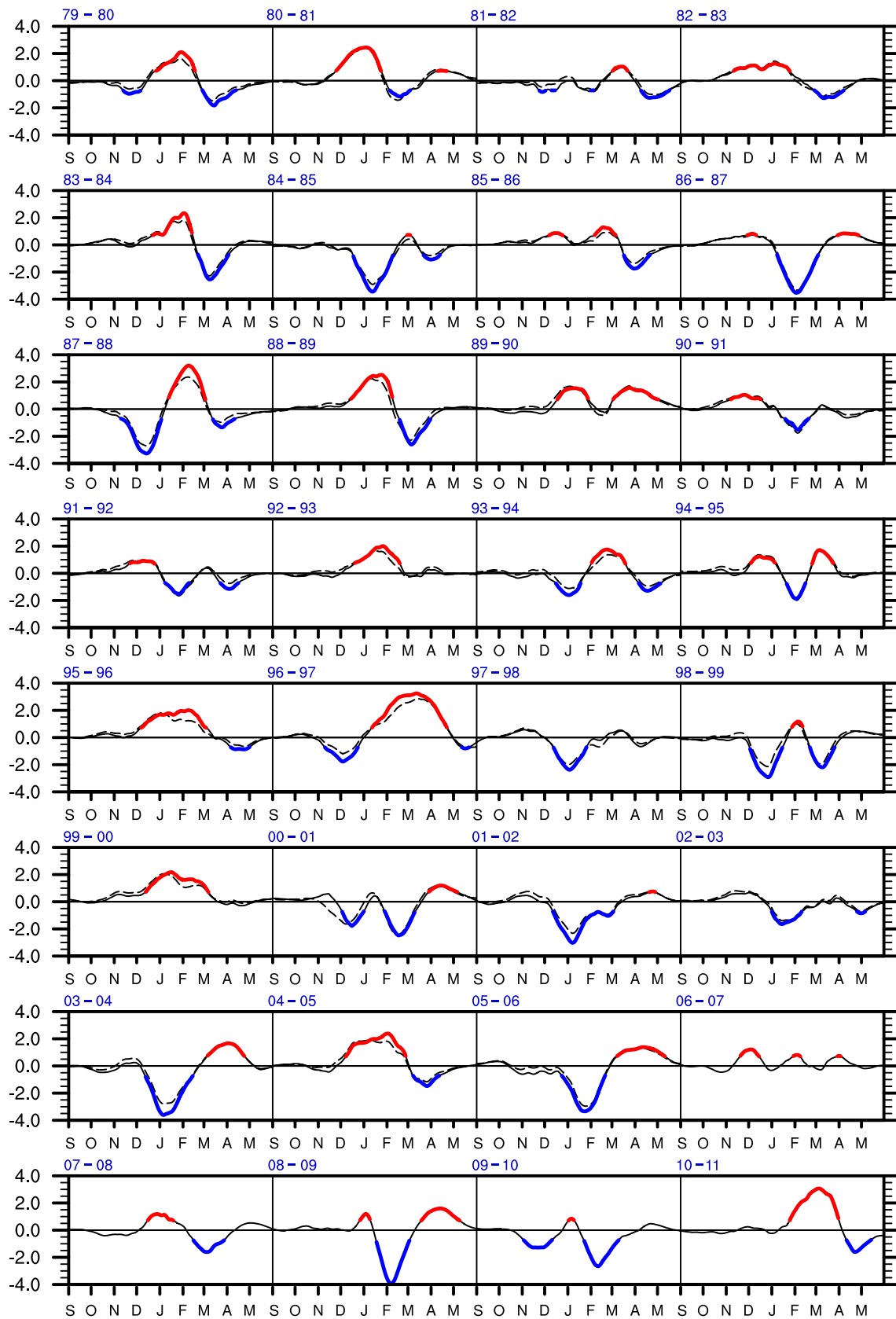
Fig. 1 Normalized first PC of the geopotential height at 10 hPa (black solid lines) and the NAM index at 10 hPa (black dashed lines). Values > 0.7 and below − 0.7 are highlighted in red and blue

correspond to eastward-tilted waves. According to the well-established baroclinic instability theory (e.g., Charney 1947; Eady 1949; Charney and Drazin 1961), only waves with a westward phase tilt with height are baroclinically unstable and able to grow in terms of amplitude, whereas other waves have to quickly decrease due to baroclinic stability. The westward phase tilt of a wave corresponds more to the growth rate of the wave amplitude than the wave amplitude itself. The dominant timescale of the westward tilting is about 2–3 weeks, much shorter that the timescale of wave amplitude in the stratosphere (Yu et al. 2018a).

The climatological mean vertical profile of wave amplitude during the 32 winters from November 1979 to March 2011 (Fig. S1a) is characterized by a remarkable increase with height. The westward tilting is positive at all pressure levels with a minimum of 6° around the mid-troposphere (Fig. S1b). The probability of the occurrence of positive values of the westward tilting index (Fig. S1c) is consistently up to 100% in the lower troposphere below 500 hPa, 95% in the stratosphere, and 87% in the mid-troposphere. These results clearly show that atmospheric motion in the extra-tropics is dominated by baroclinic waves with a westward-tilted structure throughout the atmospheric column. The weakest baroclinicity in the mid- and upper troposphere might be related to the higher occurrence of wave breaking on a synoptic scale (e.g., Prezerakos 1985; Michel and Rivière 2011).

2.4 NAM-phase-based composites

An empirical orthogonal function (EOF) was applied to the 31-day running daily 10 hPa height anomalies poleward of 20°N from September to May 1979–2011. We used the principal component (PC) of the leading EOF pattern as the index to measure the oscillation of the NAM. Figure 1 clearly shows that the index used in this study is highly consistent with the daily NAM index at 10 hPa downloaded from http://www.nwra.com/resumes/baldwin/nam.php and therefore captures the features of the temporal variations in the NAM. Hereafter, we refer to the PC1 index as the NAM index.

We followed Cai and Ren (2007) and Ren and Cai (2007) and defined positive (negative) NAM events when the daily value of the NAM index was > 0.7 (< 0.7) standard deviations of the winter season NAM index. Such a condition for detecting NAM events is loose compared with that in most previous studies, allowing a larger sample size and wider range of the key features that may affect the downward propagation. There were 38 positive NAM events (NAM$^+$) and 40 negative NAM events (NAM$^-$) during the 32-year period from 1979 to 2011 (the colored sections of the curves shown in Fig. 1). Figure 1 also shows that very few examples have a positive event closely followed by a negative event and therefore we did not stitch

the positive half-cycle of NAM events to the negative half-cycle of NAM events, as in Cai and Ren (2007). Instead, to see the features in the full cycle of a NAM event, we brought forward the starting time of a positive (negative) event to the closest day when the NAM index reached a minimum (maximum) value before the peak time of the NAM$^+$ (NAM$^-$) event. Similarly, we pushed the end-time to the day when the NAM index reached a minimum (maximum) value after the peak time of the NAM event. Then each of the NAM events was normalized by its own peak amplitude. In a few cases, the absolute values of the NAM index in the beginning and at the end of the selected cycle could possibly exceed the peak intensity of the NAM event. In these cases, we excluded those periods from the life cycle of a positive or negative NAM event.

Note that even though the NAM variability is dominated by a timescale of 3–4 months, the duration of a NAM event shows a large case-to-case variability. To fairly obtain the common spatiotemporal features of NAM events with different durations, we used a composite method based on the phase of the life cycle of a NAM event (the NAM phase composite) for easy reference. A similar method has been used by Cai and Ren (2007) and is referred to as a relative intensity based composite. First, we assume that the oscillation of the NAM resembles a cycle. For the lifecycle of NAM$^+$ events, centered at the positive peak of the NAM index, the relative amplitude of the normalized NAM index varies from − 1 to 1 and then back to − 1, similar to the cycle of the cosine function. We determine the phase (denoted as Φ) at which cosine Φ was equal to the value of the normalized NAM index, where Φ ranges from 0 to 360°. The phase evolution of NAM$^+$ events is binned into 36 intervals and each bin covers a range of 10°. In the same fashion, for NAM$^-$ events, the relative amplitude of the normalized NAM index varies from 1 to − 1 and then back to 1, similar to the cycle of the cosine function. The phase (Φ) can also be determined by cosine Φ equal to the value of the normalized NAM index. All the daily fields during the life cycles of each of the 38 NAM$^+$ and 40 NAM$^-$ events selected in this study can therefore be composited based on the phase bin they fall into. The NAM phase composites of the NAM index itself for NAM$^+$ and NAM$^-$ events (Fig. 2) confirm that such NAM phase composite analysis can faithfully capture the life cycle of NAM and help us to compare or obtain common features at specific stages of the NAM cycles despite their differences in duration.
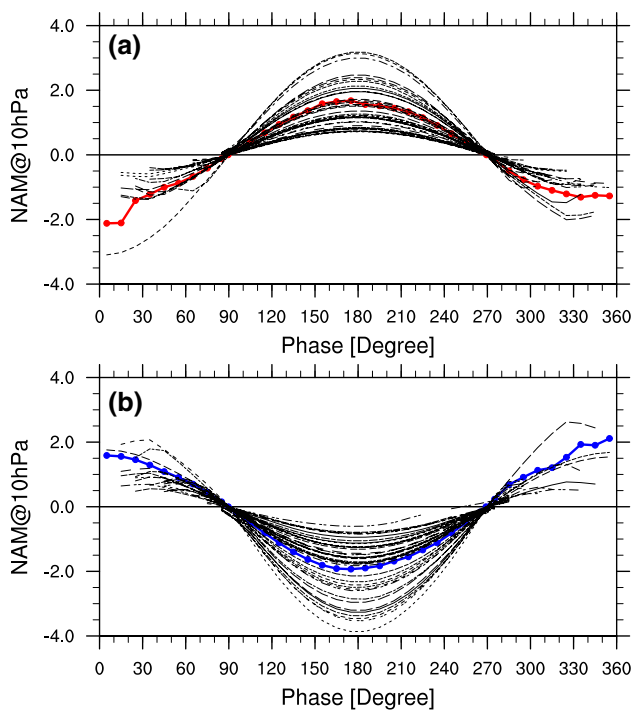
Fig. 2 Composite NAM cycle: **a** 38 positive events and **b** 40 negative events. The red and blue curves show the mean results. The ordinate represents the NAM phase composite NAM index and the abscissa is the timeline in unit of phase for the composite NAM event

3 S–T coupling variation during stratospheric NAM events from a mass circulation perspective

3.1 Case-to-case differences

We begin by inspecting the NAM phase composite anomalies of temperature (contours) in high latitudes (60–90°N) and adiabatic mass flux (shading) at 60°N during each of the 38 NAM⁺ (Fig. 3) and 40 NAM⁻ events (Fig. 4). Negative temperature anomalies in the upper layers are found during almost all the NAM⁺ events in the phase period from $\Phi = 90°$ to $\Phi = 270°$, with a maximum negative temperature anomaly at about $\Phi = 180°$ at the isentropic level of 550 K, consistent with the maximum positive values of the NAM index derived from the geopotential height at 10 hPa. The opposite features are found in the NAM⁻ events. There are, however, large case-to-case differences in the vertical structure of the polar temperature anomalies, which indicate propagating features. In some cases, temperature anomalies of the same sign appear to propagate downward to the lower troposphere and surface (e.g., NAM⁺ #4, NAM⁺ #5, NAM⁺ #9, NAM⁻ #5, and NAM⁻ #29), whereas in other cases the temperature anomalies show a structure that is vertically out of phase (e.g., NAM⁺ #1, NAM⁺ #2, NAM⁺ #12, NAM⁻ #1, NAM⁻ #8, and NAM⁻ #14), as reported in Cai

and Ren (2006, 2007). The vertical structure of some of the temperature anomalies shows tripolar features (e.g., NAM⁺ #7, NAM⁺ #26, NAM⁻ #2, and NAM⁻ #7). The existence of tripolar features suggests that even when the temperature anomalies between the stratosphere and near surface are in phase, there may still be temperature anomaly signals of the opposite sign around the mid-troposphere. This provides supporting evidence for the minimum correlation of the NAM index around the mid-troposphere with the stratospheric NAM index reported by Cai and Ren (2007).

Previous studies have suggested that the downward propagation of stratospheric circulation signals may be related to the intensity and duration of NAM events. Table 1 lists the intensity and duration of the selected NAM to determine whether there is a robust dependence of the vertical structure of the temperature anomalies on these two parameters. Here, for a NAM⁻ (NAM⁺) event, the intensity is defined as the negative (positive) peak value during the event, whereas the duration is defined as the time period when the NAM index is above (below) 0.7 (−0.7) standard deviation. Unexpectedly, we did not find a strong correspondence between the intensity and duration of the NAM events and the downward propagation of the temperature anomalies in the polar regions into the lower troposphere or even the Earth's surface. For instance, during events of relatively large intensity and long duration (e.g., NAM⁺ #1, 2, 12, and 27 and NAM⁻ #8 and 23), the temperature anomalies did not propagate down to the surface. By contrast, during relatively weak and short-lived events (e.g., NAM⁺ #4, 8, and 9 and NAM⁻ #5), the temperature anomalies propagate downward and, even during very weak events (e.g., NAM⁺ #7, NAM⁻ #24 and 32), the temperature anomalies show an in-phase relationship between the stratosphere and the near surface despite an interruption in the mid-troposphere. In addition to the variety in the vertical structure of temperature anomalies associated with NAM events, the timing (or the phase of the NAM life cycle) of the occurrence of the in-phase, out-of-phase, or tripolar vertical structure of temperature anomalies also varies from case to case.

It is noteworthy that all these various temporal and vertical patterns of temperature anomalies are found in accordance with the diverse relationship between the stratospheric sub-branch of the warm air branch, the tropospheric sub-branch of the warm air branch, and the cold air branch of the meridional mass circulation at 60°N during the period slightly in advance (see shading in Figs. 3, 4). The stronger (weaker) stratospheric branch (indicated by positive (negative) anomalies of F_{ad} in isentropic layers above 350 K), the tropospheric warm branch (indicated by positive (negative) anomalies of F_{ad} in isentropic layers around 290–350 K), and the tropospheric cold branch (indicated by negative (positive) anomalies of F_{ad} in isentropic layers below about 290 K) are always followed by positive (negative
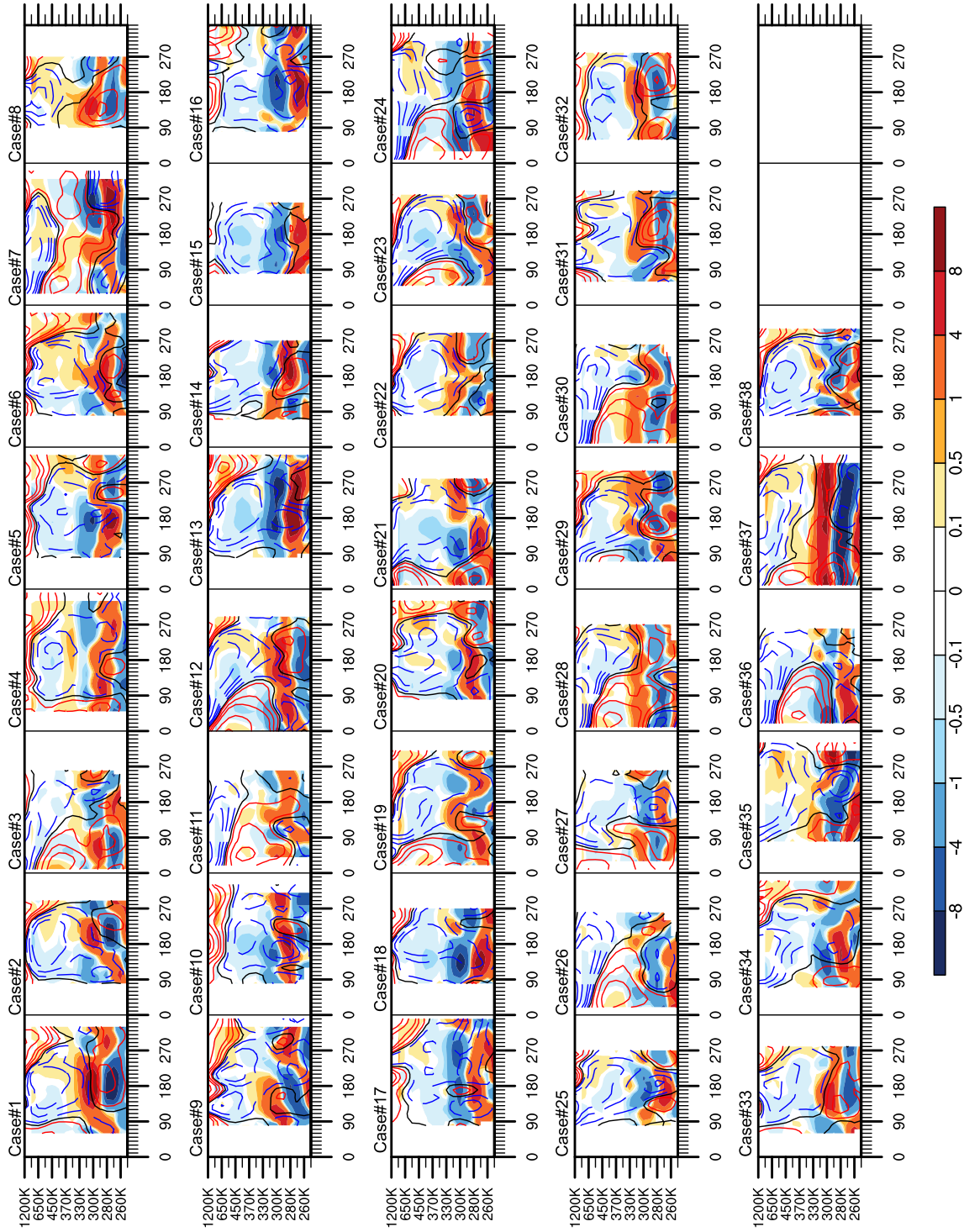
Fig. 3 Vertical phase cross-sections of 15-day running mean anomalies of temperature (units: K; contours) and adiabatic mass flux (units: 10^9 kg/s; shading) during the NAM phase composite lifecycles of the 38 NAM[+] events
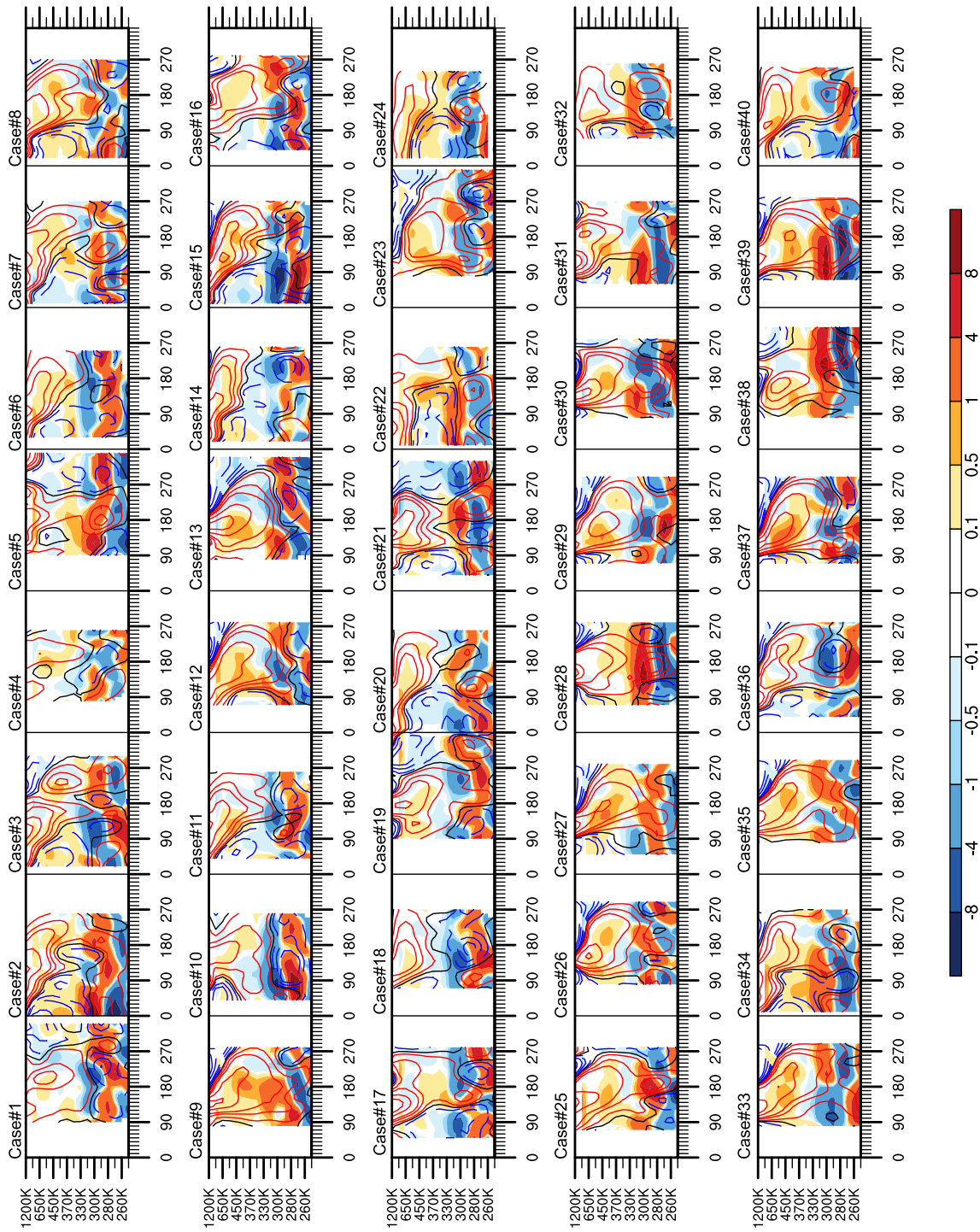
Fig. 4 Vertical phase cross-sections of 15-day running mean anomalies of temperature (units: K; contours) and adiabatic mass flux (units: 10^9 kg/s; shading) during the NAM phase composite lifecycles of the 40 NAM⁻ events

Table 1 Peak time, peak value, and duration (units: days) of positive and negative NAM events included in this study

Case no.	NAM⁺ event			Case no.	Peak time	Peak value	Duration of NAM > 0.7
	Peak time	Peak value	Duration of NAM > 0.7				
1	1980/01/30	2.10	53	21	1995/03/06	1.71	29
2	1981/01/04	2.45	61	22	1996/02/08	1.01	88
3	1981/04/16	0.73	13	23	1997/03/12	3.25	101
4	1982/03/13	1.04	23	24	1999/02/05	1.17	15
5	1983/01/05	1.25	76	25	2000/01/16	2.18	85
6	1984/02/02	2.32	53	26	2001/04/14	1.19	39
7	1985/03/02	0.74	5	27	2002/04/25	0.76	9
8	1985/12/14	0.87	19	28	2004/04/03	1.67	50
9	1986/02/18	1.29	29	29	2005/02/02	2.39	81
10	1986/12/06	0.82	13	30	2006/04/12	1.39	65
11	1987/04/08	0.85	29	31	2006/12/04	0.81	10
12	1988/02/09	3.20	50	32	2007/02/04	0.74	5
13	1989/01/25	2.52	56	33	2007/04/01	1.22	26
14	1990/01/11	1.54	42	34	2007/12/28	1.19	35
15	1990/03/25	1.57	61	35	2009/01/04	1.19	14
16	1990/11/26	1.05	41	36	2009/04/14	1.60	52
17	1991/12/10	0.92	34	37	2010/01/06	0.84	8
18	1993/01/27	2.00	61	38	2011/03/05	3.07	66
19	1994/02/22	1.75	46				
20	1994/12/16	1.24	33				

Case no.	NAM⁻ event			Case no.	Peak time	Peak value	Duration of NAM < −0.7
	Peak time	Peak value	Duration of NAM < −0.7				
1	1979/11/21	−0.97	24	21	1995/02/02	−1.86	26
2	1980/03/15	−1.83	46	22	1996/04/12	−0.86	26
3	1981/02/19	−1.17	28	23	1996/12/04	−1.77	45
4	1981/11/28	−0.83	15	24	1997/05/16	−0.81	11
5	1982/02/02	−0.71	4	25	1998/01/03	−2.38	45
6	1982/04/20	−1.26	39	26	1998/12/27	−2.92	44
7	1983/03/12	−1.29	40	27	1999/03/10	−2.19	34
8	1984/03/09	−2.55	42	28	2000/12/16	−1.78	30
9	1985/01/13	−3.44	54	29	2001/02/17	−2.48	41
10	1985/04/01	−1.08	23	30	2002/01/07	−3.02	82
11	1986/03/31	−1.75	36	31	2003/01/15	−1.64	41
12	1987/02/03	−3.53	56	32	2003/05/01	−0.85	12
13	1987/11/14	−3.27	55	33	2004/01/06	−3.61	64
14	1988/03/25	−1.35	30	34	2005/03/26	−1.48	36
15	1989/03/06	−2.61	42	35	2006/01/24	−3.34	59
16	1991/02/05	−1.52	32	36	2008/03/05	−1.61	42
17	1992/01/26	−1.51	33	37	2009/02/06	−3.95	45
18	1992/04/04	−1.15	25	38	2009/11/22	−1.28	39
19	1994/01/02	−1.60	34	39	2010/02/10	−2.65	47
20	1994/04/18	−1.29	30	40	2011/04/22	−1.60	34

temperature anomalies (shading) in the stratospheric layers, in the upper troposphere, and in the lower troposphere, respectively. We suggest that the large case-to-case variability of the vertical structure of the temperature anomalies during NAM events might be determined by the diverse relationship between the three sub-branches of the meridional mass circulation via the adiabatic transport of warm and cold air masses into and out of the polar region. This sharpens our insights into the intensity of the meridional mass circulation at 60°N when considering the downward propagation problem.

3.2 Several leading types of stratosphere–troposphere coupling during stratospheric NAM events

3.2.1 Coupling between the stratospheric warm branch and the tropospheric warm and cold branches of the meridional mass circulation

With the case-to-case observational results as a guide, we attempt to classify NAM events based on the relationships among ST, WB, and CB of the meridional mass circulation. To extract the dominant temporal evolution of the meridional mass circulation, we use EOF analysis and multi-variable EOF (MV-EOF) analysis (Wang 1992) on the NAM phase composite mean of the 15-day running mean intensity of the three branches during NAM events. Because the intensities of the WB and CB show a nearly perfect positive correlation and tend to be dominated by a much shorter timescale than the ST, we conduct a multi-variable EOF analysis on the WB and CB intensity anomalies, but a separate EOF analysis on the ST intensity anomalies during NAM events.

Figure 5 shows the EOF analysis results for the ST intensity anomalies. The first EOF pattern of the ST intensity (ST_EOF 1) accounts for $> 55\%$ of the total variance, which represents a temporal evolution from positive values before phase 210° to negative values afterwards, with a maximum value around phase 120°. The principal components of the ST_EOF 1 (ST_PC 1) are all negative for the 38 NAM$^+$ events (Fig. 5d) and positive for almost all the NAM$^-$ events, except #7 and #17 (Fig. 5e). The pronounced polarity preference of the temporal evolution pattern indicated by ST_EOF 1 shows that it is the sum of the accumulative effects of stronger (weaker) meridional mass transport into the polar stratosphere over a relatively long period. This mass transport tends to determine the increase (decrease) in air mass in the polar stratosphere and leads to more (less) warm air
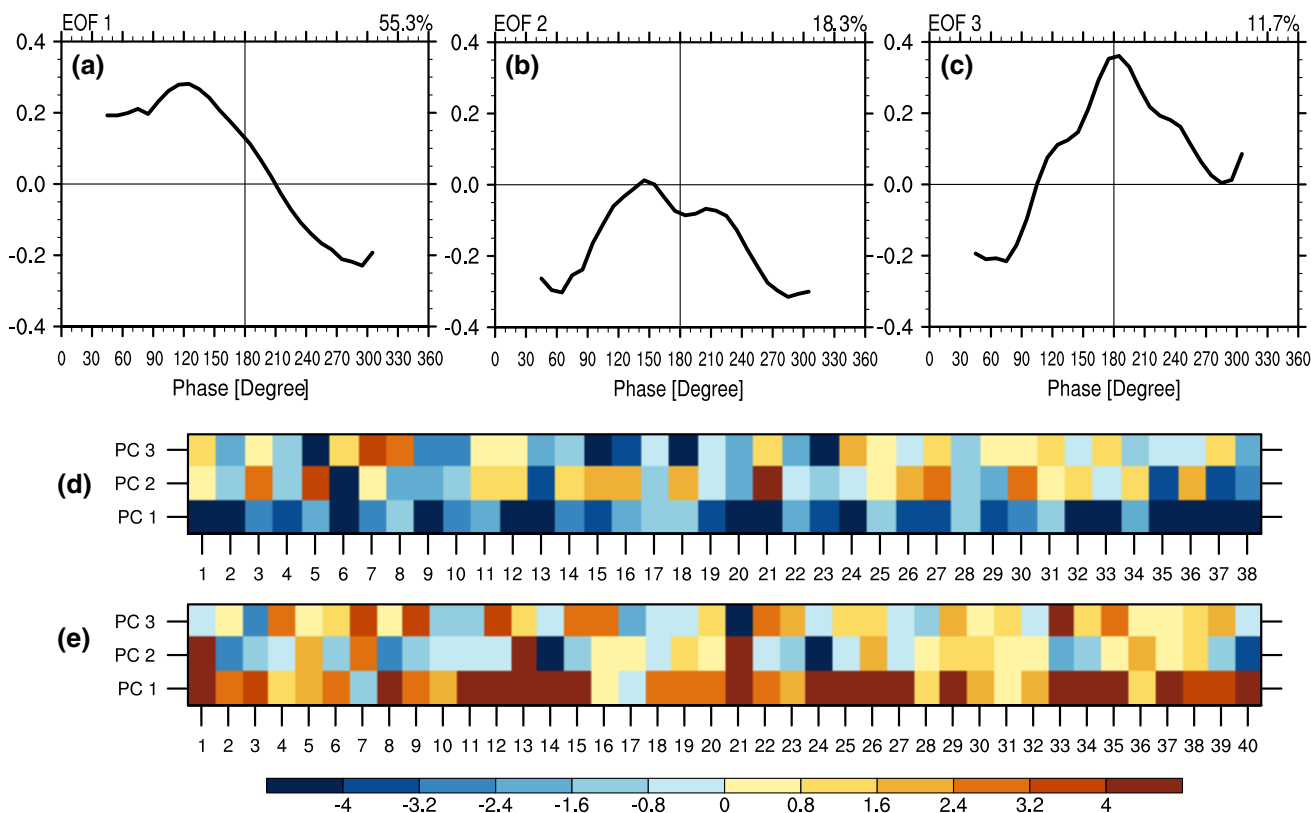

Fig. 5 **a–c** First three EOF patterns of the NAM phase composite means of the 15-day running mean anomalies of the ST intensity (normalized) during all NAM events and the three PCs for **d** NAM$^+$ events and **e** NAM$^-$ events

mass in the polar stratosphere, and thus higher (lower) pressures and temperatures, during negative (positive) NAM events. This agrees well with the 90° lead–lag relationship between the adiabatic mass transport and the variability in NAM shown by Yu et al. (2018a). The ST_EOF 2 accounts for 18.3% of the total variance, much smaller than that of ST_EOF 1, and according to the temporal evolution represented by ST_EOF 2, the role of this mode could be to slightly modify the ST intensity at the beginning and end of the NAM event. The ST_EOF 3 explains even smaller variance, and the variations in ST_EOF 3 is expected to slightly modify the ST intensity and the peak time of the ST intensity anomaly with respect to the NAM peak. The first four MV-EOF modes of co-variations of the intensities of the tropospheric warm and cold branches (WB&CB), however, show a more evenly distributed explained variance. The leading MV-EOF pattern (WBCB_EOF 1) represents the temporal evolution of the WB and CB intensities of the same sign during the entire lifecycle, with larger values from phase 120° to phase 240° and a maximum value around phase 180°. The WBCB_EOF 2 shows peak values of one sign around phase 210° (immediately after the peak time of the NAM event) and values of the opposite sign in the earlier and later periods of the NAM cycle. The temporal evolution represented by the WBCB_EOF 3 is featured by a sign reversal of the WB&CB intensity anomaly around the peak time of NAM events. WBCB_EOF 4 represents a more rapid temporal evolution of WB&CB intensity anomalies that are negative before phase 90°, but positive from phase 90° to phase 180° and then back to negative from phase 180° to phase 270°. The ST_PC 1 shows uniformly negative values in NAM$^+$, but positive values in NAM$^-$ events, whereas the PCs of WBCB_EOF 1–4 show little preference for or against the NAM polarity (Fig. 6e, f). This confirms the large variations in the relationship between the variations of the stratospheric branch of the meridional mass circulation and the tropospheric branches, which probably accounts for the diverse relationships of the temperature anomalies between the stratosphere and troposphere during NAM events, as partially seen from case to case in Figs. 3 and 4.

Table 2 shows the classification of positive and negative NAM events based on the dominant temporal evolution of the ST and the tropospheric WB&CB. We first divide all the selected NAM events into two groups based on whether the temporal evolution pattern represented by the ST_EOF 1 is dominant. For NAM$^+$ events, if the ST_EOF 1 is negative and its absolute value exceeds one-quarter of the square root of the total variance of the ST intensity, then we consider it as ST_EOF 1$^-$ dominant; otherwise, ST_EOF 1$^-$ not dominant. Similarly, for the NAM$^-$ events, if the ST_EOF 1 is positive and its absolute value exceeds one-quarter of the square root of the total variance of the ST intensity, we consider it as ST_EOF 1$^+$ dominant; otherwise, ST_EOF

1$^+$ not dominant. This study focuses on the NAM events where ST_EOF 1 is dominant by excluding NAM$^+$ events belonging to the type ST_EOF 1$^-$ not dominant (four events in total) and the NAM$^-$ events belonging to type ST_EOF 1$^+$ not dominant (seven events in total). We group the remaining 34 NAM$^+$ events and 33 NAM$^-$ events into eight categories according to the dominant pattern of the WB&CB intensity. For example, we define the events with the PC of WBCB_EOF 1 exceeding (below) $+0.7$ (-0.7) standard deviation as type WBCB_EOF 1$^+$ (WBCB_EOF 1$^-$) events. A similar definition is applied to other types of event.

The composite anomaly fields for NAM$^-$ events dominated by ST_EOF 1$^+$ belonging to type WBCB_EOF n^+ and NAM$^+$ events dominated by ST_EOF 1$^-$ belonging to type WBCB_EOF n^- are almost opposite (where $n = 1$–4). The composites for NAM$^-$ events dominated by ST_EOF 1$^+$ belonging to WBCB_EOF n^- and NAM$^+$ events dominated by ST_EOF 1$^-$ belonging to WBCB_EOF n^+ are also almost opposite. Thus in later sections we only present the difference in the NAM phase composite anomaly fields: NAM$^-$ events dominated by ST_PC 1$^+$ belonging to WBCB_EOF n^+ minus NAM$^+$ events dominated by ST_EOF 1$^-$ belonging to WBCB_EOF n^-; and NAM$^-$ events dominated by ST_EOF 1$^+$ belonging to WBCB_EOF n^- minus NAM$^+$ events dominated by ST_EOF 1$^-$ belonging to WBCB_EOF n^+. The difference in the composite fields represents a highlighted anomaly pattern in NAM$^-$ events and the opposite pattern can be expected for NAM$^+$ events. We can consider only eight types of S–T variation in view of the difference between NAM$^-$ and NAM$^+$ events (ST_EOF 1 dominant) in total: NAM$^-$_WBCB_EOF n^+/NAM$^+$_WBCB_EOF n^- and NAM$^-$_WBCB_EOF n^-/NAM$^+$_WBCB_EOF n^+ (where $n = 1$–4). In the later sections, our discussion will be mainly from the standpoint of NAM$^-$ events. These leading types of S–T variation classified based on the in-phase/out-of-phase relationship of the leading EOF modes of the temporal evolution of the WB&CB intensity anomaly with those of the ST intensity anomaly during the life cycle of NAM can well capture the main coupling situations of the three sub-branches of the meridional mass circulation at the polar circle. Such a classification method is expected to provide a clearer picture of the resultant variations of the vertical propagation of the polar mean temperature anomalies.

3.2.2 Downward propagation

Figure 7 shows the vertical-phase evolution patterns of the 15-day running mean composite anomalies of temperature over the polar region (60–90°N) and the meridional mass flux across 60°N (F_{ad}) for each of the eight S–T variation types. Next we take a close look at the S–T variations and downward propagation features for each type of NAM event.
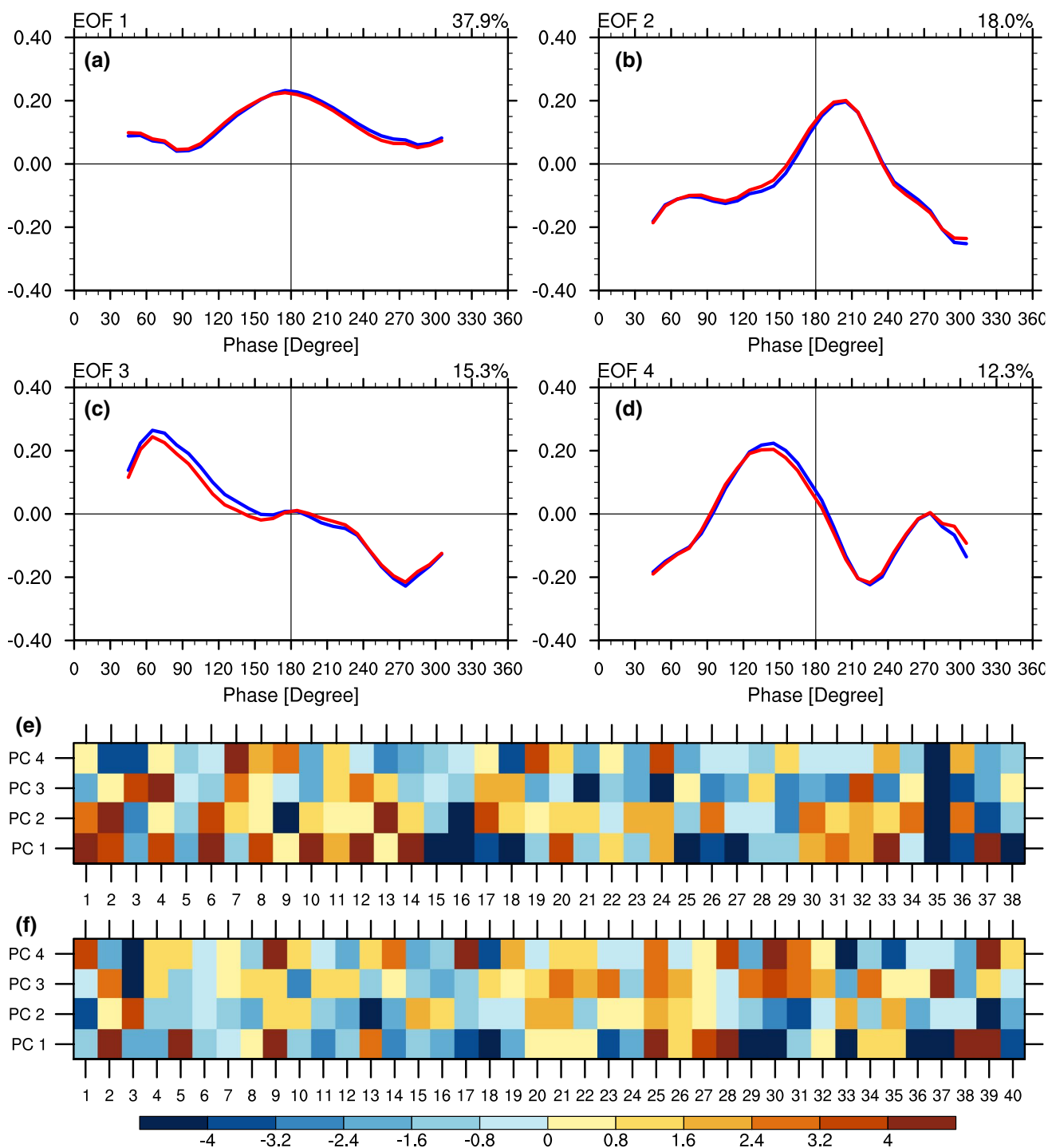
Fig. 6 a–d First four MV-EOF patterns of the NAM phase composite means of the 15-day running mean anomalies of the WB intensity (normalized, red) and the CB intensity (normalized, blue) indices during all NAM events and the four PCs for **e** NAM$^+$ events and **f** NAM$^-$ events

The NAM$^-$_WBCB_EOF 1$^+$ minus NAM$^+$_WBCB_EOF 1$^-$ composites show that for NAM$^-$ events with anomalously strong ST_EOF 1 and WBCB_EOF1 modes, the strengthening of the stratospheric cell of the mass circulation is followed immediately by the strengthening of the tropospheric cell. This is consistent with the robust in-phase relationship

between the composite F_{ad} anomalies in the stratospheric levels above 370 K and those in the upper troposphere (the isentropic layer between 280 and 330 K) as well as the robust out-of-phase relationship between F_{ad} in the stratospheric levels and that in the lower troposphere (the isentropic layer below 280 K) from phase 60° to phase 240°

Table 2 Classification of positive and negative NAM events based on the dominant temporal evolution of the NAM phase composite intensity anomalies of the stratospheric branch (ST) and the tropospheric warm and cold branches (WB&CB) of the meridional mass circulation at 60ºN

NAM	ST	WB&CB	Case no.	Total number of events
NAM$^+$	ST_EOF 1$^-$ dominant	WBCB_EOF 1$^+$	1, 2, 4, 6, 10, 12, 14, 20, 33, 37	10
		WBCB_EOF 1$^-$	15, 16, 18, 25, 26, 27, 35, 36, 38	9
		WBCB_EOF 2$^+$	1, 2, 6, 13, 17, 23, 24, 26, 30, 32, 34, 36	12
		WBCB_EOF 2$^-$	3, 9, 16, 29, 35, 37	6
		WBCB_EOF 3$^+$	3, 4, 7, 12, 13, 17, 18, 32	8
		WBCB_EOF 3$^-$	1, 6, 10, 19, 21, 23, 24, 26, 27, 29, 33, 35, 36, 37	14
		WBCB_EOF 4$^+$	7, 9, 19, 24, 33, 36	6
		WBCB_EOF 4$^-$	2, 3, 10, 13, 14, 18, 21, 23, 35, 37	10
	ST_EOF 1$^-$ not dominant	All	8, 17, 28, 31	4
NAM$^-$	ST_EOF 1$^+$ dominant	WBCB_EOF 1$^+$	2, 5, 9, 25, 27, 38, 39	7
		WBCB_EOF 1$^-$	14, 18, 23, 29, 30, 33, 37	7
		WBCB_EOF 2$^+$	3, 20, 21, 25, 33, 35	6
		WBCB_EOF 2$^-$	1, 8, 12, 13, 14, 30, 39	7
		WBCB_EOF 3$^+$	2, 21, 22, 23, 25, 26, 29, 30, 32, 34, 37	11
		WBCB_EOF 3$^-$	3, 10, 16, 33, 38	5
		WBCB_EOF 4$^+$	1, 9, 14, 19, 25, 30, 39	7
		WBCB_EOF 4$^-$	2, 3, 12, 15, 18, 29, 33, 35, 38	9
	ST_EOF 1$^+$ not dominant	All	7, 16, 17, 28, 31, 36, 40	7

(Fig. 7a, left-hand panel). The corresponding temperature anomalies (Fig. 7a, right-hand panel) show a vertically in-phase pattern appearing to propagate continuously from the stratosphere into the lower troposphere. However, this downward propagation of temperature anomalies is not a real propagation, but a result of the redistribution of the warm and cold air masses by the coupled mass circulation branches. The strengthened poleward branch in the upper isentropic layers transports more warm air into the polar region and is responsible for the higher temperature there, whereas the strengthened equatorward branch in the lower isentropic layers transports more polar cold air into the lower latitudes, thus warming the lower tropospheric polar region. By contrast, during NAM$^-$ events belonging to type WBCB_EOF 1$^-$ (i.e., when the ST_EOF 1 is anomalously strong, but the WBCB_EOF 1 is anomalously weak), the strengthened stratospheric cell is accompanied by a weakened tropospheric cell. As a result of the decoupling of the stratospheric and tropospheric cells, the propagation of temperature anomalies appears to be intercepted by statistically insignificant negative anomalies in the layer between 300 K and the near surface (Fig. 7b).

For WBCB_EOF 2$^+$ type NAM$^-$ events (Fig. 7c), the tropospheric cell of mass circulation is stronger during the negative phase of NAM (from phase 120° to phase 240°), slightly lagging the stronger stratospheric cell. As a result, the tropospheric temperature anomalies are positive immediately after the peak time, but negative in the earlier stage

of the NAM$^-$ events. Together with the unchanged temporal evolution of temperature anomalies in the stratosphere (i.e., the stronger stratospheric branch before and during the peak time of NAM$^-$ events), the vertical structure of temperature anomalies during type WBCB_EOF 2$^+$ NAM$^-$ events also shows a seemingly continuous downward propagation of positive temperature anomalies. Positive temperature anomalies reach the surface from phase 180° to phase 300°, more than a quarter cycle of the NAM after the first occurrence of statistically significant positive temperature anomalies in the upper stratosphere around phase 60°. An almost opposite spatiotemporal pattern of temperature anomalies can be seen in the mid- to lower troposphere during WBCB_EOF 2 type NAM$^-$ events (Fig. 7d). Thus a failure of the downward propagation of temperature anomalies into the lower troposphere can be observed.

During WBCB_EOF 3$^+$ type NAM$^-$ events, the tropospheric cell of mass circulation is stronger before the peak dates of NAM$^-$ events, but weaker afterwards. Such a temporal variation in tropospheric cell intensity is consistent with the variation in the stratospheric cell intensity, except that the positive peak time of the WB&CB intensity leads that of the ST intensity, whereas the negative peak time of the WB&CB intensity lags that of the ST intensity. Therefore statistically significantly positive temperature anomalies appear throughout the total column around the peak dates from phase 90° to phase 210°, indicating a simultaneous coupling of the stratosphere and troposphere
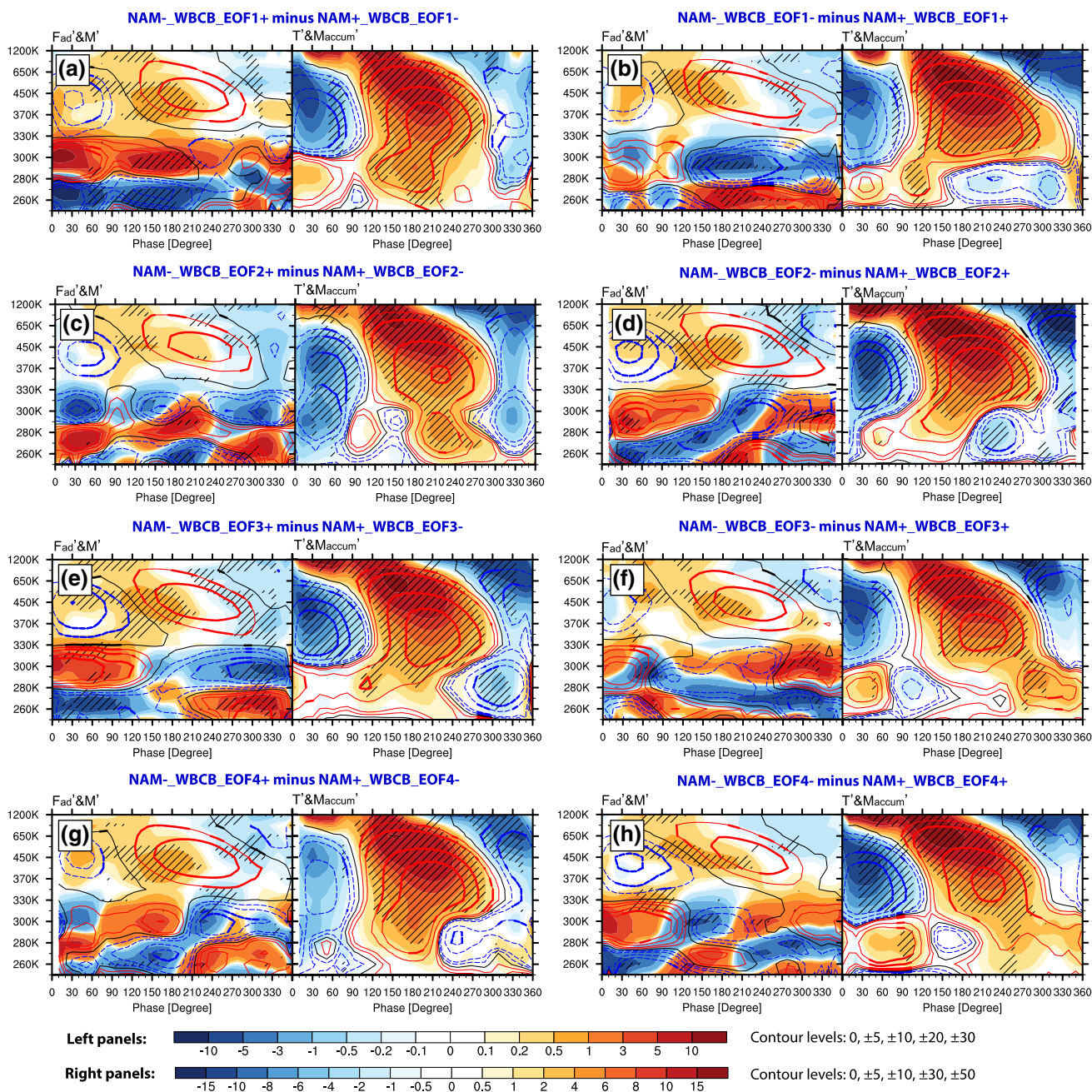
Fig. 7 Vertical phase cross-section diagrams of the 15-day running mean composite anomalies of adiabatic mass flux at 60°N (units: 10^9 kg/s, shadings) and mass 60–90°N (units: 10^{14} kg, contours) in the left-hand panels and temperature (units: K, shadings) and accumulated mass (60–90°N, units: 10^{14} kg, contours) in the right-hand panels for each of the eight stratospheric–tropospheric variation situations. Composites > 90% confidence level are hatched in the shading and thickened on the contours

in terms of temperature anomalies. The composite mean temperature anomalies become negative after phase 210° at levels below 300 K, which is followed by negative temperature anomalies at lower stratospheric levels after phase 300°. For WBCB_EOF 3$^+$ NAM$^-$ events, the significantly stronger tropospheric cell of meridional mass circulation in the period after phase 240° is immediately after the positive F_{ad} anomalies originating in the upper

stratosphere, thus even though the temperature anomalies show a vertically out-of-phase pattern around the peak time of NAM$^-$ events, we still observe a seemingly continuous vertical propagation of positive temperature anomalies. This is similar to that in WBCB_EOF 2$^+$ type events, except that the lag time of the surface signal with respect to the upper stratospheric signal is even longer.

For NAM⁻ events belonging to the type WBCB_EOF 4⁺, the tropospheric mass cell shows a variation on a shorter timescale: the tropospheric cell is significantly stronger in the phase period 90–180°, but weaker in the phase periods before 90° and 180–270°. The stronger tropospheric cell in period 90–180° is accompanied by a stronger stratospheric cell. Correspondingly, the temperature anomalies seem to be more vertically uniform, as if the temperature anomaly signal propagates rapidly down to the surface around the peak dates of NAM⁻ events. During WBCB_EOF 4⁻ type NAM⁻ events, positive temperature anomalies in the mid- to lower troposphere are found in two periods—one before phase 120° and the other after phase 210°—corresponding to the strengthening period of the tropospheric cell, whereas negative temperature anomalies are found in between. Thus the out-of-phase pattern of temperature anomalies can be found in a short period before the peak time of NAM⁻ events (phase 120° to phase 180°), but the temperature anomalies still appear to propagate downward at a rate slower than in type WBCB_EOF 2⁺ events, but quicker than in WBCB_EOF 3⁻ type events.

The close relationship between temperature anomalies and the intensity of the meridional mass fluxes can also be explained by the mass budget over the polar region. The changes in air mass in a specific layer are due to the meridional (adiabatic) mass transport into the polar region and the vertical (diabatic) mass transport across isentropic surfaces. Meridional mass transport plays a dominant part in changes in mass because the isentropic mass anomalies (contours, Fig. 7, left-hand panels) are largely of the same sign as the meridional mass flux anomalies (shading, Fig. 7, left-hand panels) at some time lags and this is confirmed by examining the diabatic mass changes (see Supplementary Material). In isentropic coordinates, the temperature at each isentropic level is directly related to the isentropic pressure, which corresponds to the total air mass stacked over this isentropic surface. This is confirmed by the almost identical distribution of the accumulated mass anomalies above each isentropic surface (contours, Fig. 7, right-hand panels) and the isentropic temperature anomalies linearly interpolated into the same isentropic level (shading, Fig. 7, right-hand panels), except the lowest level below 260 K where the accumulated mass is the total mass above surface while temperature is a linear interpolation at isentropic level 250 K. The temperature anomaly signal cannot reach the lower troposphere and surface in some types of NAM events, but can propagate to the mid- and upper troposphere. Such propagating features cannot be seen in the isentropic layer mass, which always shows a tripolar pattern with clear boundaries, one separating the stratospheric mass (around 370 K) from the tropospheric mass and the other separating the warm and cold branches (around 280 K). Based on the relationships among the mass, accumulated mass, and isentropic temperature, the fact that the lowest level that the temperature can propagate to is lower than the tropopause is mainly due to the vertically accumulative effects of the air mass above each isentropic level.

Another interesting point being made here is that regardless of S–T relation types, the surface pressure, which is proportional to the total air mass above surface indicated by the accumulated mass above the level below 260 K, tends to be in-phase with the mass anomaly in the mid-lower stratosphere in the period around and slightly after NAM peak. This again confirms the important role of stratospheric NAM signal, related with accumulated mass anomaly above tropopause, in determining the surface polar pressure related with surface NAM or AO, as at the interannual timescale reported by Yu et al. (2014). However, the surface pressure anomaly is not always consistent with the temperature anomaly, which highly depends on the CB intensity. This provides hints for the uncertainty of the correspondence between negative phase of AO and individual polar warming/mid-latitude cooling events (Thompson and Wallace 1998; Yu et al. 2015c).

Figure 8 summarizes the key features of the various anomaly fields—including the meridional mass flux, the tendency of layer mass, the accumulative mass, and temperature—for the S–T in-phase and out-of-phase scenarios during NAM⁺ and NAM⁻ events. These results provide clear evidence for the high correspondence between the specific S–T variation types in terms of the meridional mass circulation and the propagating features of temperature anomalies. The following puzzles about the downward propagation of polar stratospheric anomalies can be solved by understanding the various relationships between the stratospheric and tropospheric cells of the meridional mass circulation during the life cycle of NAM events. The puzzles are: can the stratospheric temperature anomalies propagate downward to the lower troposphere and surface; how fast is the apparent downward propagation; and is there a clear tropospheric signal at any specific time around the peak time of NAM events?

4 Wave activity corresponding to the mass circulation and S–T variation

The question still remains: what causes the variabilities in the three sub-branches of the meridional mass circulation in the extra-tropics? Johnson (1989) and subsequent studies (e.g., Cai and Shin 2014) implied that the main driving force of the meridional mass circulation in the extra-tropics is the amplifying baroclinic waves. They built a conceptual model (Johnson 1989, Fig. 10) with two isentropic layers—a lower layer and an upper layer separated by a isentropic surface—to explain the role of the amplifying baroclinic waves in
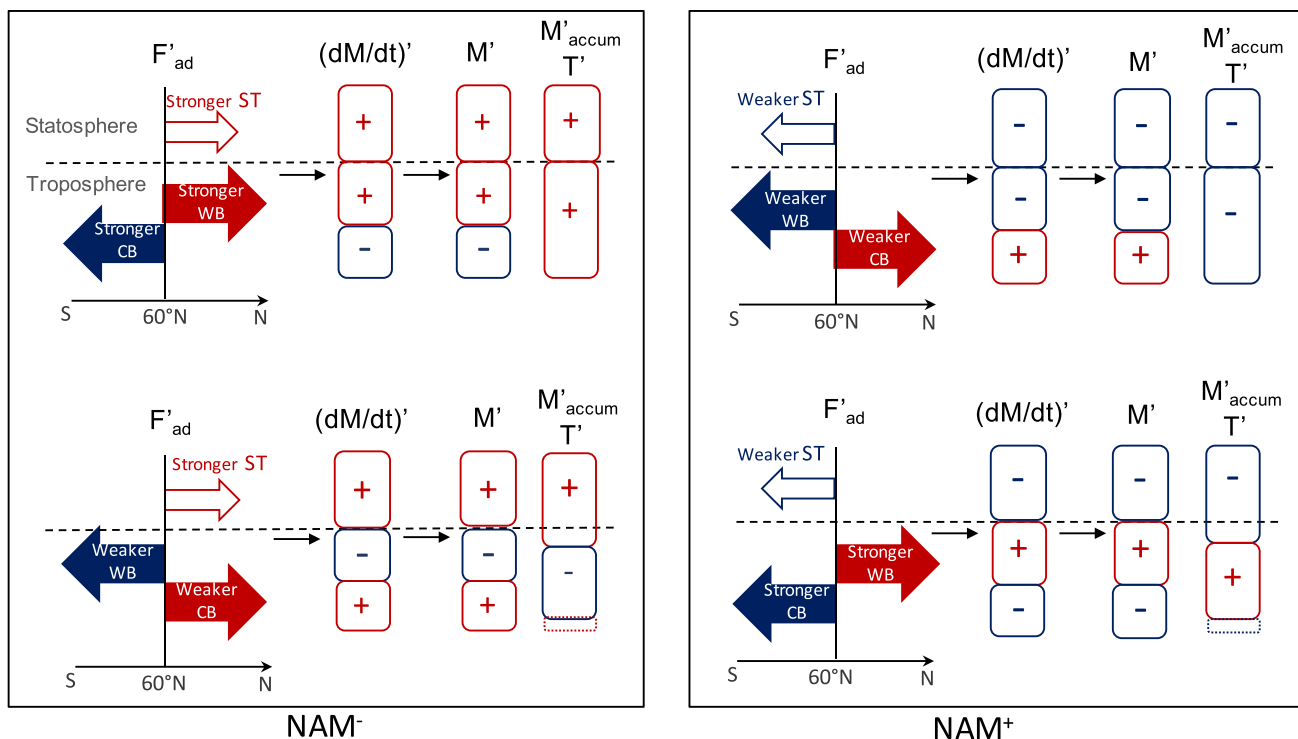
Fig. 8 Schematic diagram showing the key features of the various anomaly fields for the stratospheric–tropospheric in-phase and out-of-phase situations during NAM⁻ and NAM⁺ events. Anomaly fields include the meridional mass flux (F_{ad}) at 60°N, the tendency of layer mass over polar region (dM/dt) which is dominated by the F_{ad} at 60°N according the mass budget analysis over the polar region, and the subsequent layer mass (M), accumulative mass (M_{accum}) above the isentropic level and the polar mean isentropic temperature (dT/dt) at isentropic level. The operator ()′ indicates the anomaly of the variable. The box with a dashed frame indicates uncertainties of the sign of dT/dt anomaly, but its color denotes the sign of M_{accum} anomaly near surface (corresponding to surface pressure anomaly), which tends to be the same as the sign of the M_{accum} anomaly above stratospheric levels but opposite to the phase of stratospheric NAM

driving the meridional mass circulation in the extra-tropics. For westward-tilted unstable baroclinic waves, the longitudinal bands with northerly (southerly) winds correspond to those with a warm (cold) potential temperature, represented by a descending (lifting) of the isentropic surface below. In the upper isentropic layer, more warm air mass is transported northward by the southerly winds in front of troughs (behind ridges) than that transported southward by the northerly wind behind troughs (in front of ridges), and vice versa for the lower layer, leading to the net poleward mass transport in the upper layer and net equatorward mass transport in the lower layer. In light of Johnson's simple model for the mechanism of the formation of mass circulation in the extra-tropics, there are two factors that affect the intensity of the meridional mass circulation in the extra-tropics. One is the westward tilting of the planetary waves, which contributes to the asymmetry between the amount of air mass ahead troughs (behind ridges) in a given isentropic layer and the other is the mean amplitude of the waves along a latitudinal band, which determines the meridional wind velocity that transports the air mass poleward or equatorward. Focusing on the three sub-branches of meridional mass circulation

of interest, it is expected that a larger westward tilting near the tropopause would lead to a greater amount of air mass being transported poleward into the stratosphere, but more air mass transported equatorward in the upper troposphere, which strengthens the ST, but weakens the WB. Around the middle and lower troposphere, larger westward tilting leads to a greater air mass transported into the upper troposphere, but more air transported equatorward in the lower troposphere, strengthening both the WB and CB. Such impact of westward tilting on the changes in intensity of the three branches is stronger when it is accompanied by a larger wave amplitude. In this section, we examine the temporal evolution of the wave amplitude and westward tilting angle to confirm this conjecture and present a clearer picture of how anomalous wave activities relate to the variability of the stratospheric branch and the tropospheric warm and cold branches of the meridional mass circulation, and thus also other variables such as mass and temperature for different types of S–T variation.

Figure 9 shows the temporal evolution of the NAM phase composites of the 15-day running mean anomalies of wave amplitude and westward tilting at isobaric levels in each type
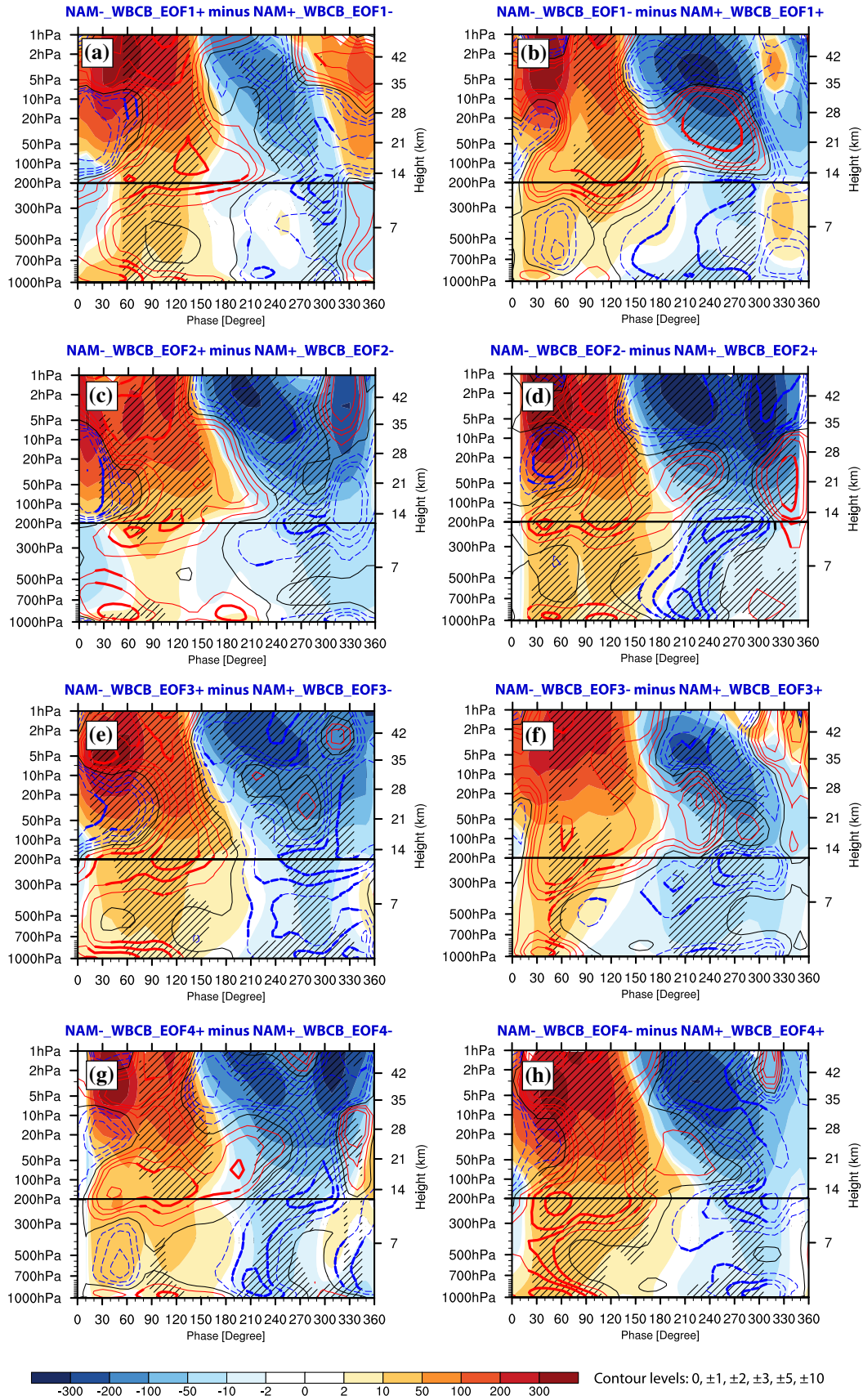
Contour levels: 0, ±1, ±2, ±3, ±5, ±10

◄**Fig. 9** Vertical phase cross-section diagrams of the 15-day running mean composite anomalies of wave amplitude (units: m, left-hand panels) and westward tilting of waves (units: degree, contours) at 60°N. Composites > 90% confidence level are hatched in the shading. In order to see the tropospheric levels clearly, we have redrawn the levels below 200 hPa with a wider vertical interval

of S–T variation. Two major common features of anomalous wave activities can be found for almost all S–T variation types. First, at stratospheric levels above 200 hPa, both the wave amplitude and westward tilting anomalies are generally positive before the NAM⁻ peak, but become negative afterwards. The timescale of the westward tilting anomaly is slightly shorter. Both the wave amplitude and westward tilting anomalies in the stratospheric levels exhibit a downward-propagating feature. A comparison of Fig. 9 with Fig. 7 shows that the downward propagation of the vertical local maxima of the positive westward tilting anomalies is in step with the propagation of positive F_{ad} anomalies in the stratosphere. This confirms that the westward-tilted waves always drive a local meridional mass circulation by causing net poleward mass transport above a specific isentropic level, but equatorward transport below. The second common feature of the composite anomaly patterns of wave amplitude and westward tilting can be seen in the troposphere at the early stage of NAM⁻ events (before phase 120°). There are always positive wave amplitude anomalies from the lower troposphere to the stratosphere, indicating stronger wave activities throughout the total column, whereas large positive westward tilting anomalies are found in the lower troposphere. Negative temperature anomalies are present in the lower and mid-stratosphere (Fig. 7, right-hand panels), equivalent to a stronger circumpolar westerly circulation. These are favorable conditions for the upward propagation of Rossby waves. This confirms the findings of previous studies on S–T variation (e.g., Ting and Held 1990; Scinocca and Haynes 1998), which showed that it is always variabilities within the troposphere—including the variability in Eurasian snow cover, the El Niño–Southern Oscillation, and atmospheric blocking (Kuroda and Kodera 1999; Cohen et al. 2001, 2002, 2007; Garfinkel et al. 2010; Kolstad and Charlton-Perez 2011)—that trigger the planetary waves in the first place before the anomalous stratospheric events leading to the possible downward impact on the troposphere.

In addition to the common features in the early stage of NAM events, the anomalous wave activities in the troposphere show a high degree of diversity. The timing of the sign reversal of the wave amplitude and westward tilting anomalies is different among different types of NAM events. Depending on whether a second round of stronger wave activities occur in the lower troposphere and near surface around of the peak time of NAM⁻ events (i.e., in addition to the first round before phase 120° mentioned above), the

eight S–T variation types can be roughly divided into two groups. For NAM⁻ events belonging to types WBCB_EOF n^+ ($n = 1$–4) plotted in Fig. 8a, c, e, g, we can see near surface a local maximum in the vertical or at least positive westward tilting anomalies, together with positive wave amplitude anomalies throughout the total column around the peak time. Specifically, after phase 120°, positive westward tilting anomalies can still be found around phase 120°–190° for the WBCB_EOF 1⁺, 120°–230° for the WBCB_EOF 2⁺ (with a maximum around phase 180°), 120°–180° for the WBCB_EOF 3⁺, and 120°–190° for the WBCB_EOF 4⁺ type anomalies. As illustrated in the schematic figure Fig. 10a, that contributes to a stronger poleward WB in the upper troposphere and equatorward CB near the surface around the peak time of NAM⁻, in phase with the stronger ST in the same period. Such coupling of the ST with WB&CB dominantly leads to the seemingly rapid downward propagation of temperature anomalies in the polar region (shadings, Fig. 7a, c, e, g, right-hand panels). For the NAM⁻ events belonging to types WBCB_EOF n^- ($n = 1$–4) plotted in Fig. 9b, d, f, h, statistically significant negative westward tilting anomalies are found in the lower troposphere during phase 150°–290° for WBCB_EOF 1⁻, 150°–250° for WBCB_EOF 2⁻, 180°–270° for WBCB_EOF 3⁻. For WBCB_EOF 4⁻, the westward tilting anomalies are also negative in the tropospheric levels since phase 130°, though not statistically significant from phase 130°–240°. As illustrated in the schematic figure Fig. 10b, the negative maxima of westward tilting anomalies near the surface lead to a weaker poleward WB and a weaker equatorward CB in the troposphere around the NAM⁻ peak, decoupled with the stronger ST. As a result, the temperature anomalies show an out-of-phase structure around the NAM⁻ peak for this group (Fig. 7b, d, f, h, right-hand panels). These results show that during the life cycle of a stratospheric NAM event, the timing of the stronger WB and CB, which make up the tropospheric mass cell, is highly dependent on the variability of the tropospheric wave itself, especially the westward tilting of waves in the lower troposphere. Although stronger waves in the stratosphere are always found before the NAM⁻ peak, it is the diverse tropospheric wave variability that leads to the coupling and decoupling of ST with WB&CB and, as a consequence, the seemingly downward propagation or nonpropagation of temperature anomalies from the stratosphere to the troposphere in the polar region.

It is interesting to see that at the later stage of the NAM⁻ events (after phase 210°), specifically around phase 270° for type WBCB_EOF 4⁺ (Fig. 9g), 300° for type WBCB_EOF 2⁻ (Fig. 9d), and type WBCB_EOF 3⁻ (Fig. 9f), 220° for type WBCB_EOF 4⁻ (Fig. 9h), when the wave amplitude is slightly weak and westward tilting anomaly does not show positive values as large as that in the early stage of NAM⁻ events or even shows close-to-zero
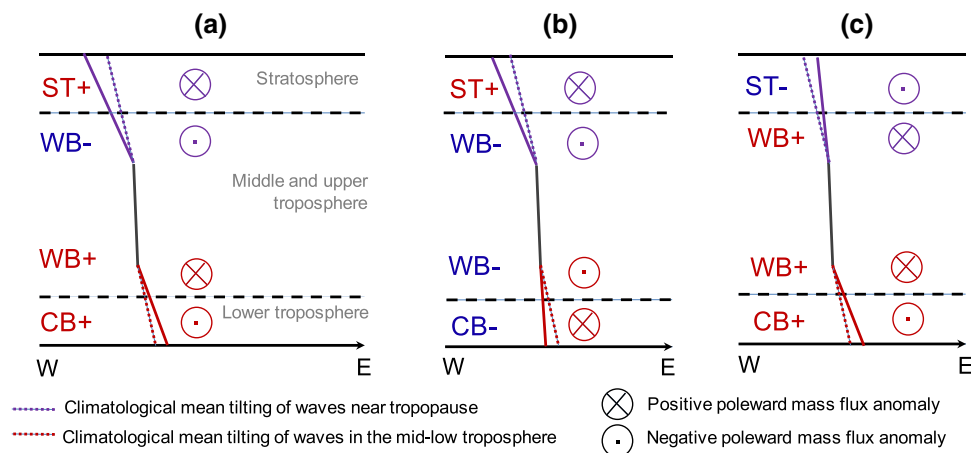
Fig. 10 Schematic diagram showing how the anomalous westward tilting of waves at the level near tropopause (purple lines) and at the level in the mid-lower troposphere (red lines) contributes to the stratospheric poleward warm branch (ST), tropospheric poleward warm branch (WB), and equatorward cold branch (CB) of the meridional mass circulation at a given latitude in mid-latitudes. **a–c** Three typical situations that can be found during the lifecycle of NAM⁻ events. Dashed horizontal lines indicate the key levels of wave tilting, approximately indicating the level at which absolute values of wave tilt reaches the local maxima in the vertical direction. "+" indicates the strengthening of the specific branch, while "−" indicates the weakening of the corresponding branch

negative values, the tropospheric cell of mass circulation is still statistically significantly stronger (left panels in Fig. 7), leading to positive temperature anomalies at tropospheric levels (right panels in Fig. 7). This could be explained by the following discussion on the possible impact of the variability of stratospheric waves on the tropospheric sub-cell of the meridional mass circulation and schematically illustrated by Fig. 10c. At the later stages of NAM⁻ events, the positive temperature anomalies (always corresponding to a weaker westerly jet) in the stratosphere tend to propagate downward to the lower stratosphere, which prohibits the upward propagation of planetary waves into the stratosphere, as indicated by the weaker westward tilting of waves and the smaller wave amplitude in the stratospheric levels shown in Fig. 9. Under such conditions, the poleward mass transport in stratospheric layers, and the equatorward transport below in the upper troposphere due to the westward-tilted waves around the tropopause, is much weaker than at the early stage of NAM⁻ events. In other words, the opposing effects of the stratospheric wave activities against the lower tropospheric wave activities on the intensity of WB in the upper troposphere is weakened at a later stage of the NAM⁻ events. As long as there is baroclinic instability in the troposphere during this period, the stratospheric state makes it easier for the tropospheric waves to strengthen the WB in the upper troposphere. The strengthened poleward mass transport leads to an increase in pressure over the polar region, strengthening the returning equatorward flow near the surface. The westward tilting of waves in the lower troposphere also contributes to a net equatorward acceleration of the mass transport in the CB near the surface. Thus, following a NAM⁻ event, tropospheric waves do not have to

be strong enough to drive a strengthened tropospheric cell, which would further lead to positive temperature anomalies in the tropospheric polar region. This is consistent with numerous previous studies showing a higher probability of warmer temperatures over the Arctic region, but cold temperatures in the mid-latitudes in the 1–2 months after weak polar vortex events (Baldwin and Dunkerton 1999, 2001; Wallace 2000; Thompson and Wallace 2001; Thompson et al. 2002; Cai 2003; Kolstad and Charlton-Perez 2011; Wei and Bao 2012; Wei et al. 2015), although the exact timing of polar warming still shows large case-to-case variations, which is dependent on the tropospheric wave activity itself.

5 Conclusions

Using the ERA-Interim reanalysis dataset covering 32 winters (September–May) in the period 1979–2011, we examine the diversity of the stratosphere–troposphere relationship from the point of view of meridional mass circulation. The normalized daily time series of the first EOF mode of the geopotential height at 10 hPa is used as the NAM index. A total of 38 positive NAM events and 40 negative NAM events have been selected during the 32 winters based on the index threshold of ±0.7. The NAM phase composite method is further applied to show the characteristic spatiotemporal evolution of the circulation anomalies during the life cycle of NAM events. Composites based on phase, instead of time, is to avoid possible temporal confusion brought about by the large case-to-case difference in event duration on the results.

A case-to-case investigation yields in-phase, out-of-phase, and tripolar vertical structures of the polar

temperature anomalies associated with NAM events. The timing of the specific thermostructure also varies from case to case. Whether the polar temperature anomalies look to propagate into the lower troposphere or even the surface is not strongly related to the intensity and duration of the NAM events as previous studies suggested, but corresponds with the dynamic heating (cooling) anomalies associated with the stratospheric portion of the warm air branch, the tropospheric portion of the warm air branch, and the cold air branch of the meridional mass circulation at 60°N.

We classify the NAM events into several leading types of stratospheric–tropospheric (S–T) relationship based on the variations in the dominant patterns of temporal evolution of the ST and WB&CB branches during the composite NAM life cycle. The dominant temporal evolution patterns of the ST and WB&CB branches are obtained utilizing EOF analysis and multi-variable EOF analysis, respectively. In the stratosphere, NAM⁻ events are always accompanied by a stronger ST before and around the peak time and a weaker ST afterwards, illustrated by the positive phase of the ST_EOF 1, and vice versa for NAM⁺ events. The EOF modes of the co-variations of the WB and CB (WBCB_EOF n, $n=1$–4), however, show a more evenly distributed explained variance, indicating that the large diversity of the relationship between the stratospheric and tropospheric branches of meridional mass circulation is mainly due to the diverse evolution patterns of the WB&CB rather than the common evolution pattern of the ST during NAM events. This study extracted eight leading S–T variation types for NAM⁻ minus NAM⁺ events in this study based on the WBCB_EOF n and presented the physical processes involved in the temporal and vertical variations of the meridional mass circulation at the polar circle to determine the vertical structure of the polar temperature anomalies and, in addition, the corresponding characteristic wave activities that drive the variability of the meridional mass circulation.

Results show that the seemingly continuous or disrupted downward propagation of the stratospheric temperature anomalies to the lower troposphere is determined by the in-phase or out-of-phase relationship between the ST and WB&CB; when and how fast the downward propagation occurs is determined by the timing of the occurrence of the in-phase or lagged in-phase relation between the ST and WB&CB. Specifically, daily changes of the air mass in each isentropic layer are dominated by adiabatic mass transport, whereas diabatic processes play only a minor role. A stronger stratospheric branch transports a greater warm air mass in the upper isentropic layers into the polar stratosphere, leading to a positive mass anomaly in this layer. By contrast, a stronger tropospheric poleward branch, accompanied by a stronger tropospheric equatorward branch at lower levels, transports a greater, relatively warm, air mass into the polar region in the upper troposphere, but more

cold air into the mid-latitudes near the surface. This leads to a positive mass anomaly in the upper troposphere and a negative anomaly at lower levels. The opposite processes are seen in weaker cells. As illustrated in Fig. 8, when ST is in phase with WB&CB, a positive (negative) mass anomaly is induced in both the stratosphere and upper troposphere, but a negative (positive) mass anomaly in the lower layers. The accumulated air mass anomaly above the corresponding isentropic surface, which is almost equivalent to the isentropic polar temperature anomaly, shows vertically consistent signs. The out of phase relation between ST and WB&CB results in a sandwich-like vertical profile of layer mass anomaly, leading to an interruption around the mid-troposphere in the accumulated air mass and temperature anomaly fields.

We further investigate the role of stratospheric and tropospheric wave activities in driving the relationships among the three sub-branches of the meridional mass circulation. For a specific isentropic level, a larger wave amplitude and stronger westward tilting (indicating baroclinic instability) contribute to stronger net poleward meridional mass fluxes in the layers above and stronger equatorward mass fluxes in the layers below along a latitude band. The NAM phase composite analysis for the wave amplitude and westward tilting anomalies for each leading type of S–T variation shows that, in the stratosphere, the wave amplitude and westward tilting at 60°N are stronger throughout the stratospheric layers before the NAM⁻ peak, but weaker afterwards, resulting in a stronger ST before the NAM⁻ peak and a weaker ST after the peak. The positive wave amplitude and westward tilting anomalies in the upper stratosphere are always accompanied by short-lived positive anomalies in the troposphere in the early stage of NAM⁻ events, representing the influence of tropospheric wave activities on the stratosphere. After the early stage, the timing of the positive westward tilting anomaly in the lower troposphere is very different among different S–T variation types of NAM events, leading to different timings of the strengthened WB&CB. For those types in which the temperature anomalies look to rapidly propagate downward, the westward tilting anomaly is positive in the lower troposphere around the peak time of NAM⁻; for those types in which the temperature anomalies propagate downward more slowly (after the peak time), the westward tilting anomaly is negative around the peak time, but positive at a later stage; for those types in which the temperature anomalies do not propagate downward, the westward tilting is out of phase both around and after the NAM⁻ peak. Drawing on what has been learned, the variations in the WB&CB, and thus the diverse timing of the in-phase or out-of-phase coupling of the ST and WB&CB, is highly dependent on the variability in the tropospheric wave itself.

Besides the results above suggesting the important role of tropospheric variability itself in leading to the various S–T

evolution during NAM events, there are also two pieces of evidence supporting that the stratosphere also exerts impact on the troposphere. First, although the isentropic polar temperature anomalies at lower isentropic levels shows high dependency on the intensity of CB, the total air mass above surface (proportional to the surface pressure) tends to have the same sign with the accumulated mass anomaly above stratospheric levels that is dominated by the anomalous meridional mass transport in the ST regardless of the S–T variation type. This suggests the important role of the air mass anomaly as well as the mass circulation variation in the stratosphere in changing the AO signature at surface and thus explains the in-phase relationship between the stratospheric NAM and the surface AO in view of mass budget over the polar region. Secondly, when stronger tropospheric waves occur in the later stage of a NAM⁻ event, the stratosphere indeed plays an important part in S–T coupling (Fig. 10c). The much weaker baroclinic instability around the tropopause at the later stage of NAM⁻ events can provide a favorable condition for the strengthening of the intensity of the WB in the upper troposphere—namely, the equatorward mass transport below (in the upper troposphere) due to the westward-tilted waves around the tropopause is much weaker than in the early stage. Thus, following a NAM⁻ event, tropospheric waves do not have to be westward tilted or strong enough to drive a strengthened tropospheric cell. The strengthened tropospheric mass cell would further lead to positive temperature anomalies in the polar region and negative temperature anomalies in the mid-latitudes at lower levels (Yu et al. 2015a, b, c). This reveals how the stratospheric variability exerts impact on the surface weather in the 1–2 months after stratospheric NAM events.

References

Baldwin MP, Dunkerton TJ (1999) Downward propagation of the Arctic oscillation from the stratosphere to the troposphere. J Geophys Res 104:30937–30946

Baldwin MP, Dunkerton TJ (2001) Stratospheric harbingers of anomalous weather regimes. Science 294:581–584

Baldwin MP, Stephenson DB, Thompson DWJ, Dunkerton TJ, Charlton AJ, O'Neill A (2003) Stratospheric memory and skill of extended-range weather forecasts. Science 301:636–640. https://doi.org/10.1126/science.1087143

Cai M (2003) Potential vorticity intrusion index and climate variability of surface temperature. Geophys Res Lett 30:1119

Cai M, Ren R-C (2006) 40–70 day meridional propagation of global circulation anomalies. Geophys Res Lett 33:L06818. https://doi.org/10.1029/2005GL025024

Cai M, Ren R-C (2007) Meridional and downward propagation of atmospheric circulation anomalies. Part I: Northern Hemisphere cold season variability. J Atmos Sci 64:1880–1901

Cai M, Shin C-S (2014) A total flow perspective of atmospheric mass and angular momentum circulations: Boreal winter mean state. J Atmos Sci 71:2244–2263

Cai M, Barton C, Shin C-S, Chagnon JM (2014) The continuous mutual evolution of equatorial waves and the Quasi-Biennial Oscillation of zonal flow in the equatorial stratosphere. J Atmos Sci 71:2878–2885

Cai M, Yu Y-Y, Deng Y, van den Dool HM, Ren R-C, Saha S, Wu X-R, Huang J (2016) Feeling the pulse of the stratosphere: an emerging opportunity for predicting continental-scale cold air outbreaks one month in advance. Bull Am Meteorol Soc 97:1475–1489

Charney JG (1947) The dynamics of long waves in a baroclinic westerly current. J Meteorol 4:135–163

Charney JG, Drazin PG (1961) Propagation of planetary-scale disturbances from the lower into the upper atmosphere. J Geophys Res 66:83–109

Cohen J, Saito K, Entekhabi D (2001) The role of the Siberian high in Northern Hemisphere climate variability. Geophys Res Lett 28:299–302

Cohen J, Salstein D, Saito K (2002) A dynamical framework to understand and predict the major Northern Hemisphere mode. Geophys Res Lett 29:1412. https://doi.org/10.1029/2001GL014117

Cohen J, Barlow M, Kushner P, Saito K (2007) Stratosphere–troposphere coupling and links with Eurasian land surface variability. J Clim 20:5335–5343

Coughlin K, Tung KK (2005) Tropospheric wave response to decelerated stratosphere seen as downward propagation in northern annular mode. J Geophys Res 110:D01103. https://doi.org/10.1029/2004JD004661

Dee DP et al (2011) The ERA-Interim reanalysis: configuration and performance of the data assimilation system. Q J R Meteorol Soc 137:553–597

Domeisen DIV, Sun LT, Chen G (2013) The role of synoptic eddies in the tropospheric response to stratospheric variability. Geophys Res Lett 40:4933–4937

Eady ET (1949) Long waves and cyclone waves. Tellus 1:33–52

ECMWF (2012) ERA Interim, daily. European Centre for Medium-Range Weather Forecasts. Subset used: 1 November 1979–28 February 2011. http://apps.ecmwf.int/datasets/data/interim-full-daily/. Accessed 1 July 2012

Gallimore RG, Johnson DR (1981) The forcing of the meridional circulation of the isentropic zonally averaged circumpolar vortex. J Atmos Sci 38:583–599. https://doi.org/10.1175/1520-0469(1981)038,0583:TFOTMC.2.0.CO;2

Garfinkel CI, Hartmann DL, Sassi F (2010) Tropospheric precursors of anomalous Northern Hemisphere stratospheric polar vortices. J Clim 23:3282–3299

Geller MA, Alpert JC (1980) Planetary wave coupling between the troposphere and the middle atmosphere as a possible sun-weather mechanism. J Atmos Sci 37:1197–1214

Gerber EP, Orbe C, Polvani LM (2009) Stratospheric influence on the tropospheric circulation revealed by idealized ensemble forecasts. Geophys Res Lett 36:L24801. https://doi.org/10.1029/2009GL040913

Hardiman SC et al (2011) Improved predictability of the troposphere using stratospheric final warmings. J Geophys Res 116:D18113. https://doi.org/10.1029/2011JD015914

Hardiman SC, Butchart N, Hinton TJ, Osprey SM, Gray LJ (2012) The effect of a well-resolved stratosphere on surface climate:

differences between CMIP5 simulations with high and low top versions of the Met office climate model. J Clim 25:7083–7099

Harnik N, Lindzen RS (2001) The effect of reflecting surfaces on the vertical structure and variability of stratospheric planetary waves. J Atmos Sci 58:2872–2894

Hines CO (1974) A possible mechanism for the production of Sun-weather correlations. J Amos Sci 31:589–591

Hitchcock P, Simpson IR (2014) The downward influence of stratospheric sudden warmings. J Atmos Sci 71:3856–3876

Hitchcock P, Shepherd TG, Manney GL (2013) Statistical characterization of arctic polar-night jet oscillation events. J Clim 26:2096–2116. https://doi.org/10.1175/JCLI-D-12-00202.1

Holton JR (2004) An introduction to dynamic meteorology, Intl Geophys Ser, 4th edn. Academic Press and Elsevier, San Diego

Iwasaki T, Mochizuki Y (2012) Mass-weighted isentropic zonal mean equatorward flow in the Northern Hemispheric winter. SOLA 8:115–118. https://doi.org/10.2151/sola.2012-029

Iwasaki T, Shoji T, Kanno Y, Sawada M, Takaya K, Ujiie M (2014) Isentropic analysis of polar cold air mass streams in the Northern Hemispheric winter. J Atmos Sci 71:2230–2243. https://doi.org/10.1175/JAS-D-13-058.1

Johnson DR (1989) The forcing and maintenance of global monsoonal circulations: an isentropic analysis. Adv Geophys 31:43–316

Kodera K, Kuroda Y (1990) Downward propagation of upper stratospheric mean zonal wind perturbation to the troposphere. Geophys Res Lett 17:1263–1266

Kodera K, Kuroda Y (2000a) Stratospheric sudden warmings and slowly propagating zonal-mean zonal wind anomalies. J Geophys Res 105:12351–12359

Kodera K, Kuroda Y (2000b) Tropospheric and stratospheric aspects of the Arctic Oscillation. Geophys Res Lett 27:3349–3352

Kolstad EW, Charlton-Perez AJ (2011) Observed and simulated precursors of stratospheric polar vortex anomalies in the Northern Hemisphere. Clim Dyn 37:1443–1456

Kuroda Y (2002) Relationship between the polar-night jet oscillation and the annular mode. Geophys Res Lett 29:1240. https://doi.org/10.1029/2001GL013933

Kuroda Y, Kodera K (1999) Role of planetary waves in the stratosphere–troposphere coupled variability in the northern hemisphere winter. Geophys Res Lett 26:2375–2378

Limpasuvan V, Thompson DWJ, Hartmann DL (2004) The life cycle of the Northern Hemisphere sudden stratospheric warmings. J Clim 17:2584–2596

Limpasuvan V, Hartmann DL, Thompson DWJ, Jeev K, Yung YL (2005) Stratosphere–troposphere evolution during polar vortex intensification. J Geophys Res 110:D24101. https://doi.org/10.1029/2005JD006302

Michel C, Rivière G (2011) The link between Rossby wave breakings and weather regime transitions. J Atmos Sci 68:1730–1748

Nakagawa KI, Yamazaki K (2006) What kind of stratospheric sudden warming propagates to the troposphere? Geophys Res Lett 33:L04801. https://doi.org/10.1029/2005GL024784

Pauluis O, Czaja A, Korty R (2008) The global atmospheric circulation on moist isentropes. Science 321:1075–1078

Perlwitz J, Graf HF (2001) Troposphere–stratosphere dynamic coupling under strong and weak polar vortex conditions. Geophys Res Lett 28:271–274

Perlwitz J, Harnik N (2004) Downward coupling between the stratosphere and troposphere: the relative roles of wave and zonal mean processes. J Climate 17:4902–4909

Plumb RA, Semeniuk K (2002) Downward migration of extratropical zonal wind anomalies. J Geophys Res 108:D7. https://doi.org/10.1029/2002JD002773 4223

Prezerakos NG (1985) Synoptic scale atmospheric wave break down at 500 hPa over Europe during cold seasons. Arch Meteorol Geophys Bioclimatol Ser A 34:145–158

Ren RC, Cai M (2007) Meridional and vertical out-of-phase relationships of temperature omalies associated with the Northern Annular Mode variability. Geophys Res Lett 34:L07704

Rind D, Perlwitz J, Lonergan P (2005) AO/NAO response to climate change: 1. Respective influences of stratospheric and tropospheric climate changes. J Geophys Res 110:D12107. https://doi.org/10.1029/2004JD005103

Runde T, Dameris M, Garny H, Kinnison DE (2016) Classification of stratospheric extreme events according to their downward propagation to the troposphere. Geophys Res Lett 43:6665–6672

Scaife AA, Knight JR, Vallis GK, Folland CK (2005) A stratospheric influence on the winter NAO and North Atlantic surface climate. Geophys Res Lett 32:L18715. https://doi.org/10.1029/2005GL023226

Schmitz G, Grieger N (1980) Model calculations of the structure of planetary waves in the upper troposphere and lower stratosphere as a function of the wind field in the upper stratosphere. Tellus 32:207–214

Scinocca JF, Haynes PH (1998) Dynamical forcing of stratospheric waves by the tropospheric circulation. J Atmos Sci 55:2361–2392

Shin CS (2012) A hybrid Lagrangian/Eulerian view of the global atmospheric mass circulation: seasonal cycle. Ph.D. dissertation, Florida State University, p 144

Shindell DT, Miller RL, Schmidt GA, Pandolfo L (1999) Simulation of recent northern winter climate trends by greenhouse gas forcing. Nature 399:452–455

Shoji T, Kanno Y, Iwasaki T, Takaya K (2014) An isentropic analysis of the temporal evolution of East Asian cold air outbreaks. J Clim 27:9337–9348. https://doi.org/10.1175/JCLI-D-14-00307.1

Sigmond M, Scinocca JF, Kharin VV, Shepherd TG (2013) Enhanced seasonal forecast skill following stratospheric sudden warmings. Nat Geosci 6:98–102. https://doi.org/10.1038/ngeo1698

Simmons A, Uppala S, Dee D, Kobayashi S (2006) ERA-Interim: new ECMWF reanalysis products from 1989 onwards. ECMWF Newsletter, No. 110, ECMWF, Reading, pp 26–35

Song Y, Robinson WA (2006) Dynamical mechanisms for stratospheric influences on the troposphere. J Atmos Sci 61:1711–1725

Thompson DW, Wallace JM (1998) The Arctic Oscillation signature in the wintertime geopotential height and temperature fields. Geophys Res Lett 25:1297–1300

Thompson DWJ, Wallace JM (2001) Regional climate impacts of the Northern Hemisphere annular mode. Science 293:85–89. https://doi.org/10.1126/science.1058958

Thompson DWJ, Baldwin MP, Wallace JM (2002) Stratospheric connection to Northern Hemisphere wintertime weather: implications for prediction. J Clim 15:1421–1428

Thompson DWJ, Baldwin MP, Solomon S (2005) Stratosphere–troposphere coupling in the Southern Hemisphere. J Atmos Sci 62:708–715. https://doi.org/10.1175/JAS-3321.1

Ting MF, Held IM (1990) The stationary wave response to a tropical SST anomaly in an idealized GCM. J Atmos Sci 47:2546–2566

Townsend RD, Johnson DR (1985) A diagnostic study of the isentropic zonally averaged mass circulation during the First GARP Global Experiment. J Atmos Sci 42:1565–1579, https://doi.org/10.1175/1520-0469(1985)042,1565:ADSOTI.2.0.CO;2

Wallace JM (2000) North Atlantic Oscillation/annular mode: two paradigms—one phenomenon. Q J R Meteorol Soc 126:791–805

Wang B (1992) The vertical structure and development of the ENSO anomaly mode during 1979–1989. J Atmos Sci 49:698–712

Wei K, Bao Q (2012) Projections of the East Asian winter monsoon under the IPCC AR5 scenarios using a coupled model: IAP_FGOALS. Adv Atmos Sci 29:1200–1214

Wei K, Takahashi V, Chen W (2015) Long-term changes in the relationship between stratospheric circulation and East Asian winter monsoon. Atmos Sci Lett 16:359–365

Yoden S, Yamaga T, Pawson S, Langematz U (1999) A composite analysis of the stratospheric sudden warmings simulated in a perpetual January integration of the Berlin TSM GCM. J Meteorol Soc Jpn 77:431–445

Yu YY, Ren RC, Hu JG, Wu GX (2014) A mass budget analysis on the interannual variability of the polar surface pressure in the winter season. J Atmos Sci 71:3539–3553

Yu YY, Cai M, Ren RC, Van den Dool HM (2015a) Relationship between warm air mass transport into upper polar atmosphere and cold air outbreaks in winter. J Atmos Sci 72:349–368

Yu YY, Ren RC, Cai M (2015b) Dynamical linkage between cold air outbreaks and intensity variations of the meridional mass circulation. J Atmos Sci 72:3214–3232

Yu YY, Ren RC, Cai M (2015c) Comparison of the mass circulation and AO indices as indicators of cold air outbreaks in northern winter. Geophys Res Lett 42:2442–2448

Yu YY, Cai M, Ren RC (2018a) A stochastic model with a low-frequency amplification feedback for the stratospheric northern annular mode. Clim Dyn 50:3757–3773

Yu YY, Cai M, Ren RC, Rao J (2018b) A closer look at the relationships between meridional mass circulation pulses in the stratosphere and cold air outbreak patterns in Northern Hemispheric winter. Clim Dyn. https://doi.org/10.1007/s00382-018-4069-7, in press

Yu YY, Cai M, Shi CH, Ren RC (2018c) On the linkage among strong stratospheric mass circulation, stratospheric sudden warming, and cold weather events. Mon Weather Rev 146:2717–2739

Zhang Q, Shin CS, Van den Dool H, Cai M (2013) CFSv2 prediction skill of stratospheric temperature anomalies. Clim Dyn 41:2231–2249. https://doi.org/10.1007/s00382-013-1907-5

Zhou S, Miller AJ, Wang J, Angell JK (2002) Downward propagating temperature anomalies in the preconditioned polar stratosphere. J Clim 15:781–792